GSA Data Repository Item 2017315
Supplemental Text and Figures

Jacobson, C.E., Hourigan, J.K., Haxel, G.B., and Grove, M., 2017, Extreme latest Cretaceous–Paleogene low-angle subduction: Zircon ages from Orocopia Schist at Cemetery Ridge, southwestern Arizona,USA: Geology, doi:10.1130/G39278.1

Contents

Appendix DR1: Zircon U-Pb sample preparation, analytical technique, and data reduction

Zircon Separations

Rock samples were crushed using a jaw crusher and Bico disc mill. The crushed material was sieved and the finer-than-150 μ fraction was processed to obtain zircon. First, a magnet was used to remove iron filings. The material was then panned to concentrate heavy minerals. The concentrate was processed with methylene iodide in a separatory funnel. The methylene iodide sink was further purified using a Frantz L-1 isodynamic separator.

Sample Mounts

Unknowns were sprinkled onto double-sided tape mounted on a glass plate. A piece of film with a 2.5 mm circular hole punched through it was used as a mask to limit the extent of each sample. Standards were mounted manually using a sharp pick. Unknowns and standards were confined to a circular area with a diameter of 15 mm. Grains were embedded in epoxy using a ring form with a diameter of 25 mm. The mount was ground and polished to expose grain interiors.

LA-ICP-MS Analysis Procedures

U-Pb Analyses were conducted at the University of California of California using a single-collector Element XR magnetic-sector ICP-MS and a Photon Machines Analyte.H 193 nm ArF excimer laser equipped with a Helex 2-volume laser ablation cell. Procedures follow those described by Sharman et al. (2013) and Dumitru et al. (2016). Here we present a condensed description of the procedures with an emphasis on those aspects unique to our analytical session and/or particularly salient to the current discussion.

We used a relatively small laser spot size (18 μ) due to small grain size of several of our samples. This compares to the 25–26 μ sizes used by Sharman et al. (2013) and Dumitru et al. (2016).

Analysis points are preprogrammed and the system runs unattended. A maximum of 600 spots can be obtained per session (~200 standards and ~400 unknowns), a constraint placed by the software.

We used zircon standard Temora II (416.8 ± 1.3 Ma; Black et al., 2004) as the primary age standard. Five analyses were collected on Temora at the beginning and end of the session, and one analysis after every fifth unknown. Secondary age standards were also run at the beginning and end of each session and at various intervals throughout the session. Secondary standards consisted of FC5Z from Duluth Gabbro (1099 Ma), Mt. Dromedary Monzonite (99 Ma), and Plešovice (337 Ma). Madder (525 Ma) was utilized as a standard for abundances of U and Th.

Each analysis begins with ~20 seconds of counting with the laser off to obtain background counts, followed by ~20 seconds of lasing. An interval of ~20 seconds after lasing allows for washout and for positioning of the next analysis spot and focusing.

Data Reduction and Plotting

Data reduction (except for calculation of common Pb corrections) was conducted in Iolite 2.5 running under Igor Pro 6.3 (Paton et al., 2011).

In Iolite, all results for a given analytical session are plotted on a single graph with time along the horizontal axis. Any of the measured or calculated parameters (e.g. count rates of U, Th, or the various lead isotopes, isotope ratios, or ages) can be displayed (see Fig. DR2).

Iolite assigns each analysis a default "integration," which represents the portion of the analysis over which Iolite calculates average count rates, isotope ratios, ages, etc. We set the default integration to start ~1.5 seconds after the onset of laser ablation and end ~5.5 seconds prior to the termination of laser ablation, which yields an integration length of ~13 seconds. In other words, we did not use data from the deeper part of the pit, where the downhole correction may be less accurate. Nonetheless, the portion of the trace following the end of the integration provides a qualitative indication of $^{206}Pb/^{238}U$ age in the deeper part of the pit.

During data processing, each default integration was examined and the start and/or end time adjusted to exclude zones of high common Pb, inclusions, "drill-throughs," or other problematic parts of an analysis. For analyses that reveal multiple age domains, we added one or more integrations in addition to the default integration in order to resolve the age variations. Conversely, in some cases we deleted even the single default integration for analyses that were clearly not sampling zircon or that otherwise seemed uninterpretable. Alternatively, bad analyses can be retained at this stage and eliminated later from the final data tables.

Errors reported throughout are propagated errors (Paton et al., 2011). These take into account the internal variability of individual analyses, as well as an external precision obtained by treating each primary standard analysis as an unknown.

The output from Iolite was not corrected for common Pb. For ages <800 Ma, for which we report $^{206}Pb/^{238}U$ age, we used Isoplot 3.75 (Ludwig, 2012) in Excel 2003 to perform a ^{207}Pb correction (Age7corr function), which assumes concordance between the $^{207}Pb/^{235}U$ and $^{206}Pb/^{238}U$ ages. For ages >800 Ma, the odds of discordance between $^{207}Pb/^{235}U$ and $^{206}Pb/^{238}U$ ages is much greater than for young ages, so it is not practical to use the ^{207}Pb correction. However, we were unable to perform a ^{204}Pb correction owing to inability to resolve interference with ^{204}Hg. This same problem led Dumitru et al. (2016) to use uncorrected $^{207}Pb/^{206}Pb$ ages for results >1000 Ma. This is reasonable considering that common Pb contamination, on average, will have less impact on older than younger analyses. Following Dumitru et al. (2016), we used uncorrected $^{207}Pb/^{206}Pb$ ages for ages >800 Ma. This approach is validated by the systematic nature of our results for ages > 800 Ma (see caption for Fig. 5). However, as described elsewhere (Figs. DR5 and DR6), several of our samples exhibit abnormally high common Pb, and this may impact young zircon or zircon with low U. We attempted to ameliorate this problem by eliminating analyses or parts of analyses exhibiting high count rates for mass 204. Furthermore, results for the Miocene igneous samples, almost all of which include only a single zircon age population, imply that the ^{207}Pb correction adequately accounts for even high levels of common Pb. The

^{207}Pb correction, however, will not yield correct ages for zircon affected by both common lead and inheritance (see caption for Fig. DR5).

Probability distributions were calculated using the Excel 2003 spreadsheet provided by the Arizona LaserChron Center (https://docs.google.com/document/d/1MYwm8GcdYFOsfNV62B6PULb_-g2r1AS3vmm4gHMOFxg/preview). Probability distributions were plotted using the scientific graphing package Origin.

References

Black, L.P., Kamo, S.L., Allen, C.M., Davis, D.W., Aleinikoff, J.N., Valley, J.W., Mundil, R., Campbell, I.H., Korsch, R.J., Williams, I.S., and Foudoulis, C., 2004, Improved 206Pb/238U microprobe geochronology by the monitoring of a trace-element-related matrix effect: SHRIMP, ID-TIMS, ELAICP-MS and oxygen isotope documentation for a series of zircon standards: Chemical Geology, v. 205, p. 115–140.

Dumitru, T.A., Elder, W.P., Hourigan, J.K., Chapman, A.D., Graham, S.A., and Wakabayashi, J., 2016, Four Cordilleran paleorivers that connected Sevier thrust zones in Idaho to depocenters in California, Washington, Wyoming, and, indirectly, Alaska: Geology, v. 44, p. 75–78, doi:10.1130/G37286.1.

Ludwig, K.R., 2012, User's manual for Isoplot 3.75: A Geochronological Toolkit for Microsoft Excel: Berkeley Geochronology Center, Special Publication 5, 75 p.

Paton, C., Hellstrom, J.C., Paul, B., Woodhead, J.D., and Hergt, J.M., 2011, Iolite: Freeware for the visualization and processing of mass spectrometric data: Journal of Analytical Atomic Spectrometry, v. 26, p. 2508–2518, doi:10.1039/c1ja10172b.

Sharman, G.R., Graham, S.A., Grove, M., and Hourigan, J.K., 2013, A reappraisal of the early slip history of the San Andreas fault, central California, USA: Geology, v. 41, p. 727–730, doi: 10.1130/G34214.1.

Figure DR1. Cumulative (A) and relative (B–I) probability distributions of zircon U-Pb ages for individual Orocopia Schist metasandstone samples from Cemetery Ridge (1 page of graphs).

Samples are ordered from north (top of figure) to south (bottom of figure) (see Fig. 1B of the main text for sample locations).

Line colors in (A) correspond to the fill colors in (B–I). Sample CR33 is further distinguished in (A) by dashed line type.

Note horizontal-axis scale break at 300 Ma. For the cumulative probability diagram (A), the vertical scale ranges from 0 to 100% both to the left and right of the horizontal-axis scale break. For the relative probability diagrams (B–I), vertical scales differ to the left and right of the horizontal-axis break such that equal area represents equal probability throughout the graph.

Analyses deemed discordant according to the criteria described in the section on data reduction are not plotted.

As described in the main manuscript, ages <65 Ma are considered to be metamorphic.

Early Miocene ages were observed in four samples. These indicate either fine igneous veinlets in the samples or hydrothermal growth of zircon. The Miocene grains were not included in the probability diagrams of Cemetery Ridge samples in the main manuscript (Figs. 2A and 2B).

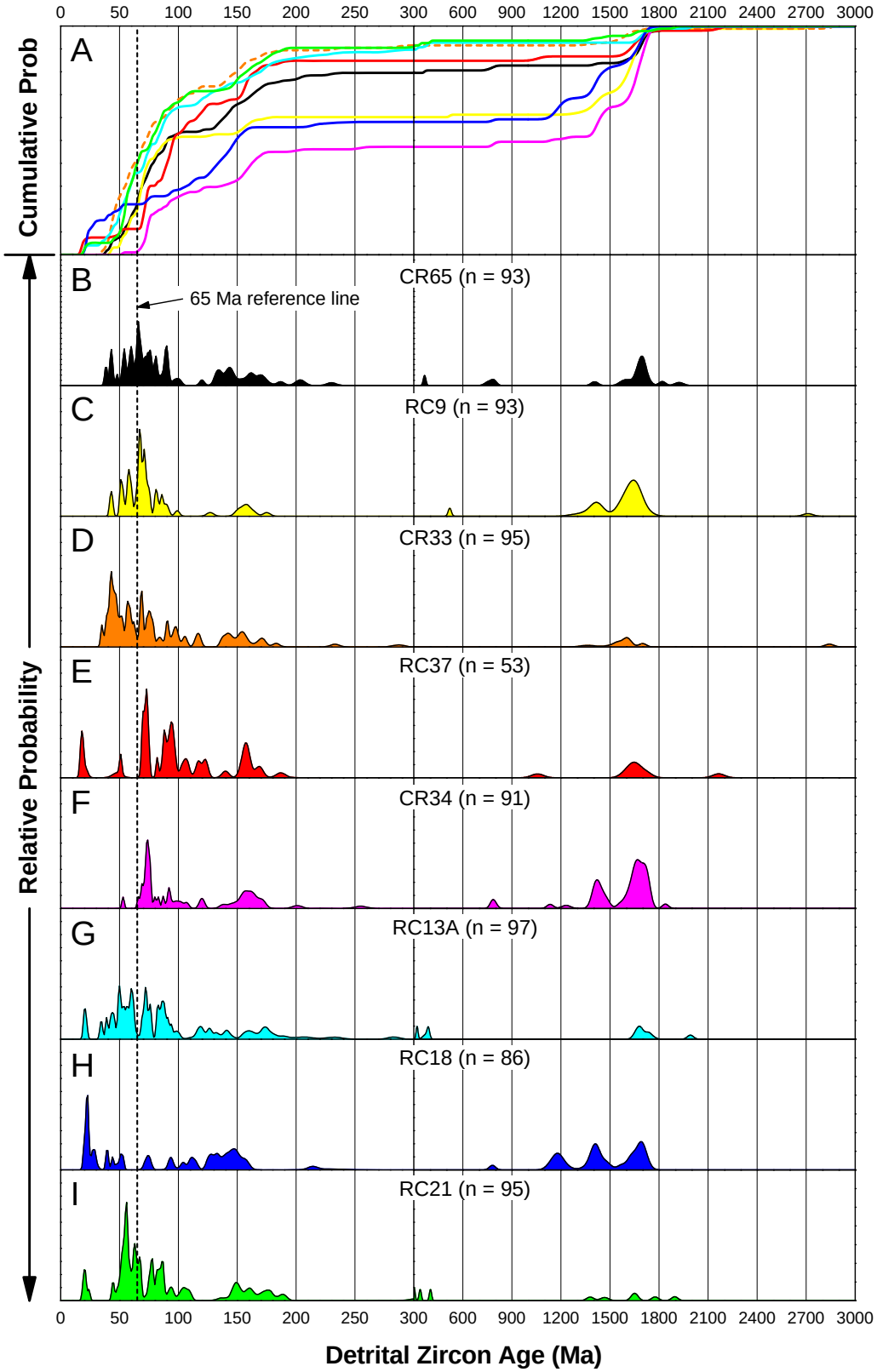
0 50 100 150 200 250 300 600 900 1200 1500 1800 2100 2400 2700 3000
A
Cumulative Prob
B
CR65 (n = 93)
65 Ma reference line
C
RC9 (n = 93)
D
CR33 (n = 95)
E
RC37 (n = 53)
F
CR34 (n = 91)
G
RC13A (n = 97)
H
RC18 (n = 86)
I
RC21 (n = 95)
Relative Probability
0 50 100 150 200 250 300 600 900 1200 1500 1800 2100 2400 2700 3000
Detrital Zircon Age (Ma)

Figure DR2. Depth profiles from Iolite (see Appendix DR1) of laser-ablation–inductively coupled plasma–mass spectrometry (LA-ICP-MS) data for zircons that yielded $^{206}Pb/^{238}U$ ages <70 Ma for at least part of the analysis (5 pages of graphs).

The graphs presented here represent screen captures from Iolite that include only the time of laser ablation and ~1 second preceding and following the period of ablation (i.e., most of the period of background counting and the washout period between analyses are omitted). The screen captures were compiled in Adobe Illustrator. Each analysis is labeled with the sample number and analysis (grain) number; e.g., CR33-04 in the upper left graph on the first page of figures indicates the 4th grain (spot) analyzed in sample CR33.

The traces on each graph show counts per second for U (purple), Th (green), and ^{204}Pb (gold) and $^{206}Pb/^{238}U$ age (red). The latter is not corrected for common Pb, as this calculation was performed outside of Iolite using Isoplot 3.75 (Ludwig, 2012). A vertical-axis scale is shown only for $^{206}Pb/^{238}U$ age, as the absolute count rates for U, Th, and ^{204}Pb are not considered important to the purposes here. Nonetheless, the scales for U and Th counts are the same; hence, their ratio can be estimated approximately from the relative heights of the traces. The count rates do not take into account fractionation of Th relative to U, but this ratio is close to 1.0. Note that, for constant abundance of U or Th, absolute count rates decrease downhole.

Integrations (see Appendix DR1) appear in the plots as black rectangles. The integrations are here shown associated with the trace for $^{206}Pb/^{238}U$ age, but could be assigned to any of the traces.

Each integration is assigned a number, which is indicated in the graphs to the upper right of the integration box. These labels are generated automatically by Iolite. Integration number starts at "1" for each sample (i.e., each rock; e.g., CR33 versus CR65). Hence, integration and analysis number will initially coincide. However, if extra integrations are added, or the single default analysis deleted, integration and analysis number can diverge. This is the case for most of our samples, as we created extra integrations for many analyses. A corollary is that we typically obtained more ages (integrations) per sample than spots (grains) analyzed, although some of those ages were ultimately discarded due to discordance.

Each integration shown here also includes a label indicating $^{206}Pb/^{238}U$ age. These labels were added manually in Adobe Illustrator. They were typically placed to the left of the integration box, but in some cases were situated elsewhere to enhance legibility. These ages have been corrected for common Pb in Isoplot 3.75 using the ^{207}Pb method (Ludwig, 2012; see Appendix DR1). The corrected ages differ from the apparent (uncorrected) age of the $^{206}Pb/^{238}U$ trace where common Pb is high. For example, integration 50 in grain CR65-46 (fifth graph from the left in the upper row) has a corrected age of 66 Ma, whereas the trace for that part of the analysis has an uncorrected age of ca. 90 Ma (see vertical scale at the left margin of the figure). The elevated common Pb for this sample is evident in the trace for ^{204}Pb (gold).

For each sample, plots of individual analyses are arranged according to the age of the youngest integration from each analysis, increasing from left to right and top to bottom. In addition, some analyses include a segment after the end of the default integration period (see Appendix DR1),

that, based on the $^{206}Pb/^{238}U$ trace, has an age <70 Ma. However, without an integration, we do not have a calculated age for these segments. These analyses are typically arranged at the end of the series of plots for each sample. Examples of the latter are common in sample RC13A.

A number of grains exhibit an age at the beginning of the analysis consistent with detrital ages from other bodies of Orocopia Schist (i.e., latest Cretaceous or older; Grove et al., 2003; Jacobson et al., 2011), followed by a Paleogene age later in the analysis (e.g., analysis CR33-01 – 8th plot from the left in the top row). We interpret these as cases of the laser drilling from a grain interior (exposed by polishing) into a metamorphic rim on the bottom of the grain. In some grains, an inferred detrital core is succeeded by one Paleogene zone, in turn followed by a younger Paleogene zone (e.g., CR65-03 – 8th plot from the left in the top row). In contrast, some grains exhibiting Paleogene ages show no variation in age over the course of the analysis. The latter results suggest substantial growth of new zircon during the Paleogene. Finally, other grains display $^{206}Pb/^{238}U$ ages that vary continuously over the course of the analysis (i.e., they do not exhibit a plateau) or alternate back and forth between apparent metamorphic and detrital ages. This is not surprising considering that many analyses were initiated toward the margins of the polished surface of the grain. In these cases, the laser may be ablating a mixture of core and rim material throughout the analysis.

References

Grove, M., Jacobson, C.E., Barth, A.P., and Vućić, A., 2003, Temporal and spatial trends of Late Cretaceous–early Tertiary underplating of Pelona and related schist beneath southern California and southwestern Arizona, *in* Johnson, S.E., Patterson, S.R., Fletcher, J.M., Girty, G.H., Kimbrough, D.L., and Martin-Barajas, A., eds., Tectonic evolution of northwestern Mexico and the southwestern USA: Geological Society of America Special Paper 374, p. 381–406, doi:10.1130/0-8137-2374-4.381.

Jacobson, C.E., Grove, M., Pedrick, J.N., Barth, A.P., Marsaglia, K.M., Gehrels, G.E., and Nourse, J.A., 2011, Late Cretaceous-early Cenozoic tectonic evolution of the southern California margin inferred from provenance of trench and forearc sediments: Geological Society of America Bulletin, v. 123, p. 485–506, doi:10.1130/B30238.1.

Ludwig, K.R., 2012, User's manual for Isoplot 3.75: A Geochronological Toolkit for Microsoft Excel: Berkeley Geochronology Center, Special Publication 5, 75 p.

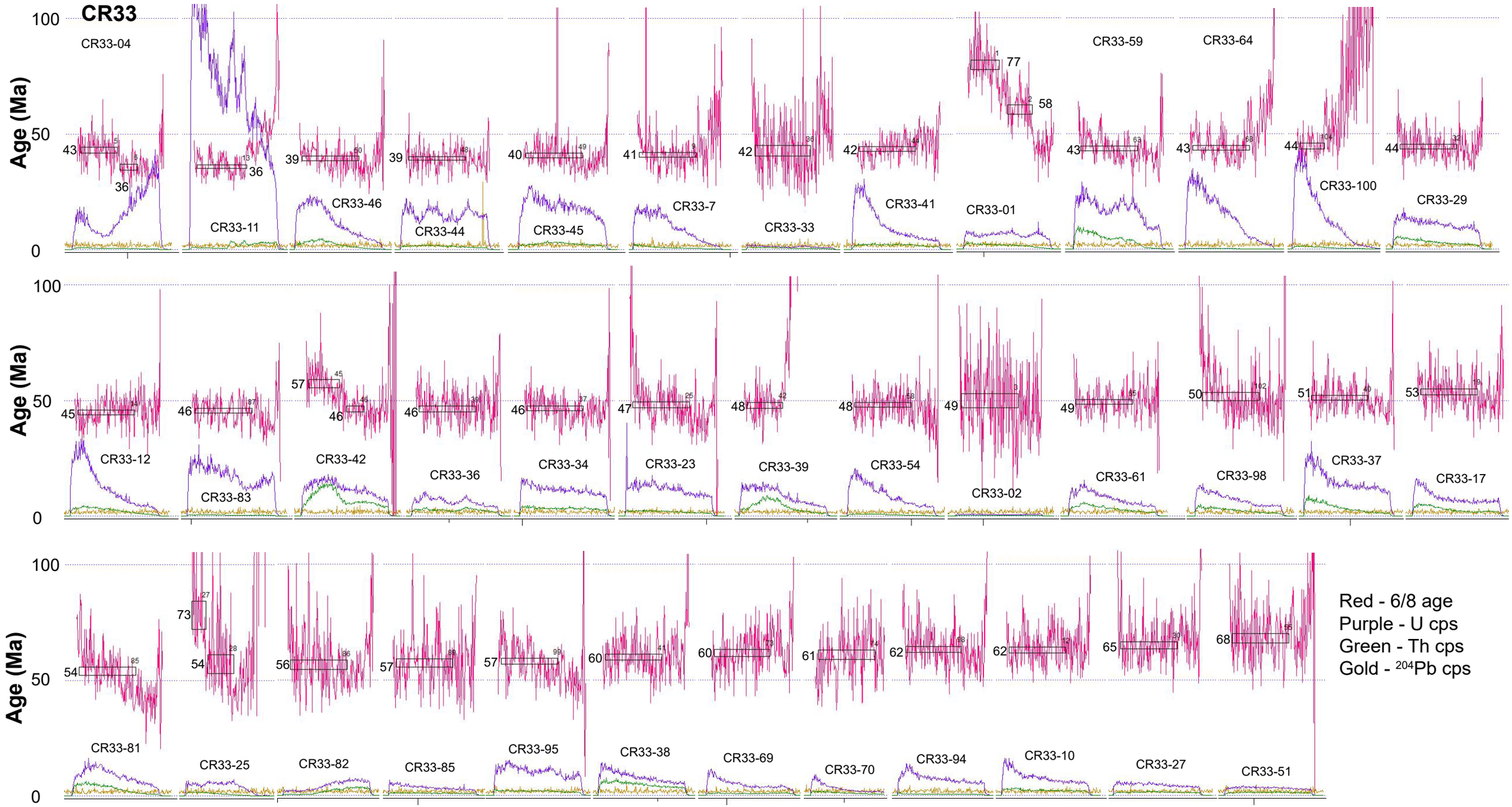

Small numbers to upper right of integration boxes indicate integration number
Larger numbers generally to the left of the integration box indicate age in Ma (207 corrected)
Traces for 6/8 age (red) are not corrected for common lead

Time (each analysis spans ~22 seconds)

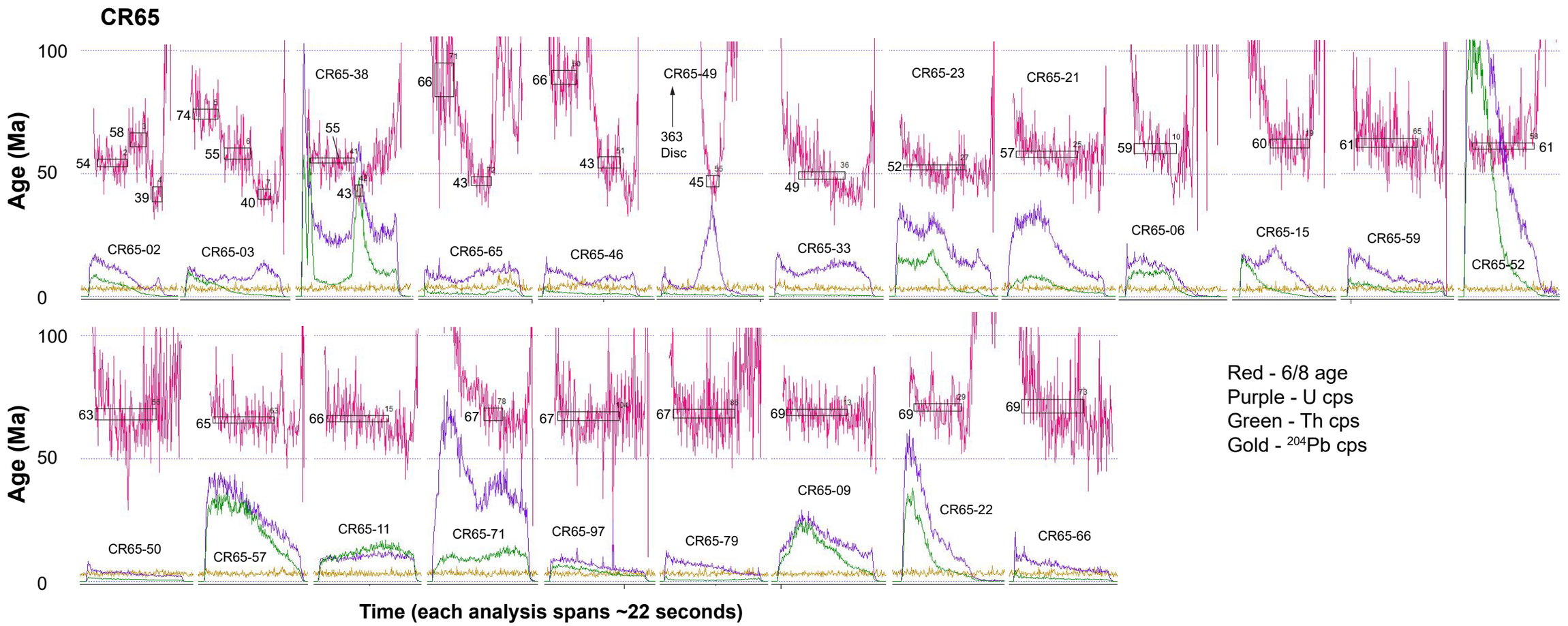

Small numbers to upper right of integration boxes indicate integration number
Larger numbers generally to the left of the integration box indicate age in Ma (207 corrected)
Traces for 6/8 age (red) are not corrected for common lead

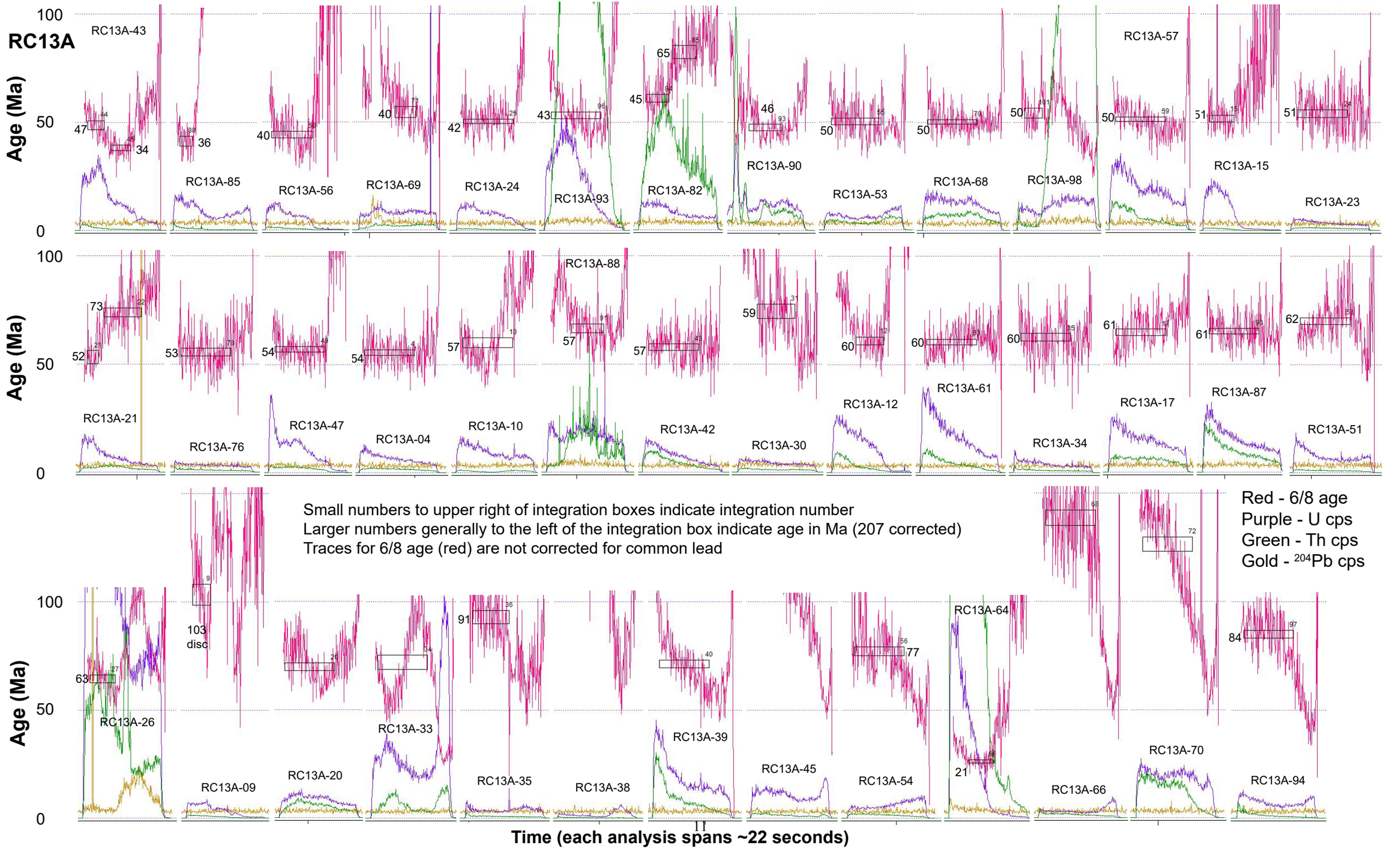
RC13A
Age (Ma)
100
50
0
RC13A-43
RC13A-85
RC13A-56
RC13A-69
RC13A-24
RC13A-93
RC13A-82
RC13A-90
RC13A-53
RC13A-68
RC13A-98
RC13A-57
RC13A-15
RC13A-23
RC13A-21
RC13A-76
RC13A-47
RC13A-04
RC13A-10
RC13A-88
RC13A-42
RC13A-30
RC13A-12
RC13A-61
RC13A-34
RC13A-17
RC13A-87
RC13A-51
RC13A-26
103
disc
RC13A-09
RC13A-20
RC13A-33
RC13A-35
RC13A-38
RC13A-39
RC13A-45
RC13A-54
RC13A-64
RC13A-66
RC13A-70
RC13A-94
Small numbers to upper right of integration boxes indicate integration number
Larger numbers generally to the left of the integration box indicate age in Ma (207 corrected)
Traces for 6/8 age (red) are not corrected for common lead
Red - 6/8 age
Purple - U cps
Green - Th cps
Gold - 204Pb cps
Time (each analysis spans ~22 seconds)

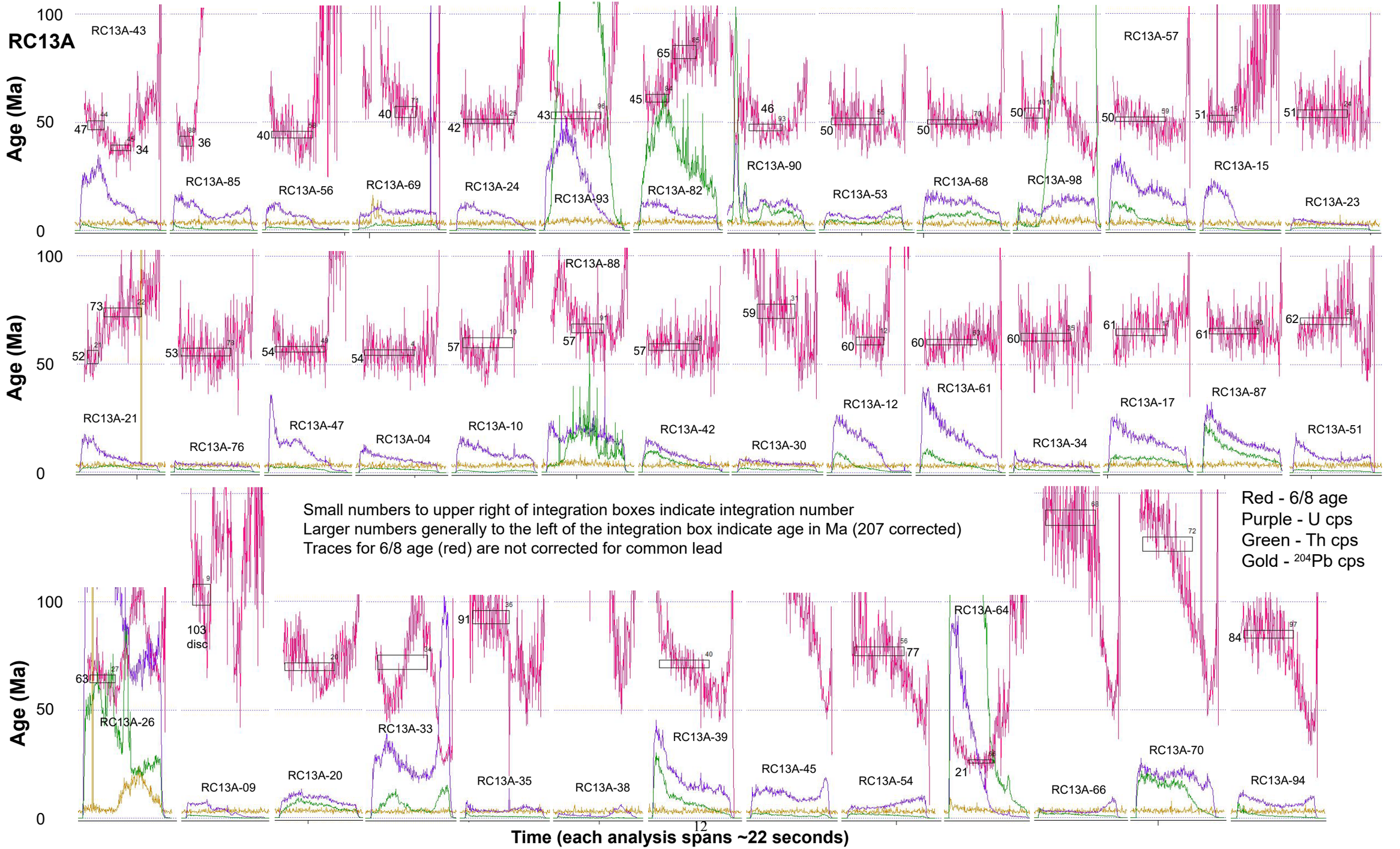
RC13A
Age (Ma)
100
50
0
RC13A-43
RC13A-85
RC13A-56
RC13A-69
RC13A-24
RC13A-93
RC13A-82
RC13A-90
RC13A-53
RC13A-68
RC13A-98
RC13A-57
RC13A-15
RC13A-23
RC13A-21
RC13A-76
RC13A-47
RC13A-04
RC13A-10
RC13A-88
RC13A-42
RC13A-30
RC13A-12
RC13A-61
RC13A-34
RC13A-17
RC13A-87
RC13A-51
103
disc
RC13A-26
RC13A-09
RC13A-20
RC13A-33
RC13A-35
RC13A-38
RC13A-39
RC13A-45
RC13A-54
RC13A-64
RC13A-66
RC13A-70
RC13A-94
Small numbers to upper right of integration boxes indicate integration number
Larger numbers generally to the left of the integration box indicate age in Ma (207 corrected)
Traces for 6/8 age (red) are not corrected for common lead
Red - 6/8 age
Purple - U cps
Green - Th cps
Gold - 204Pb cps
Time (each analysis spans ~22 seconds)

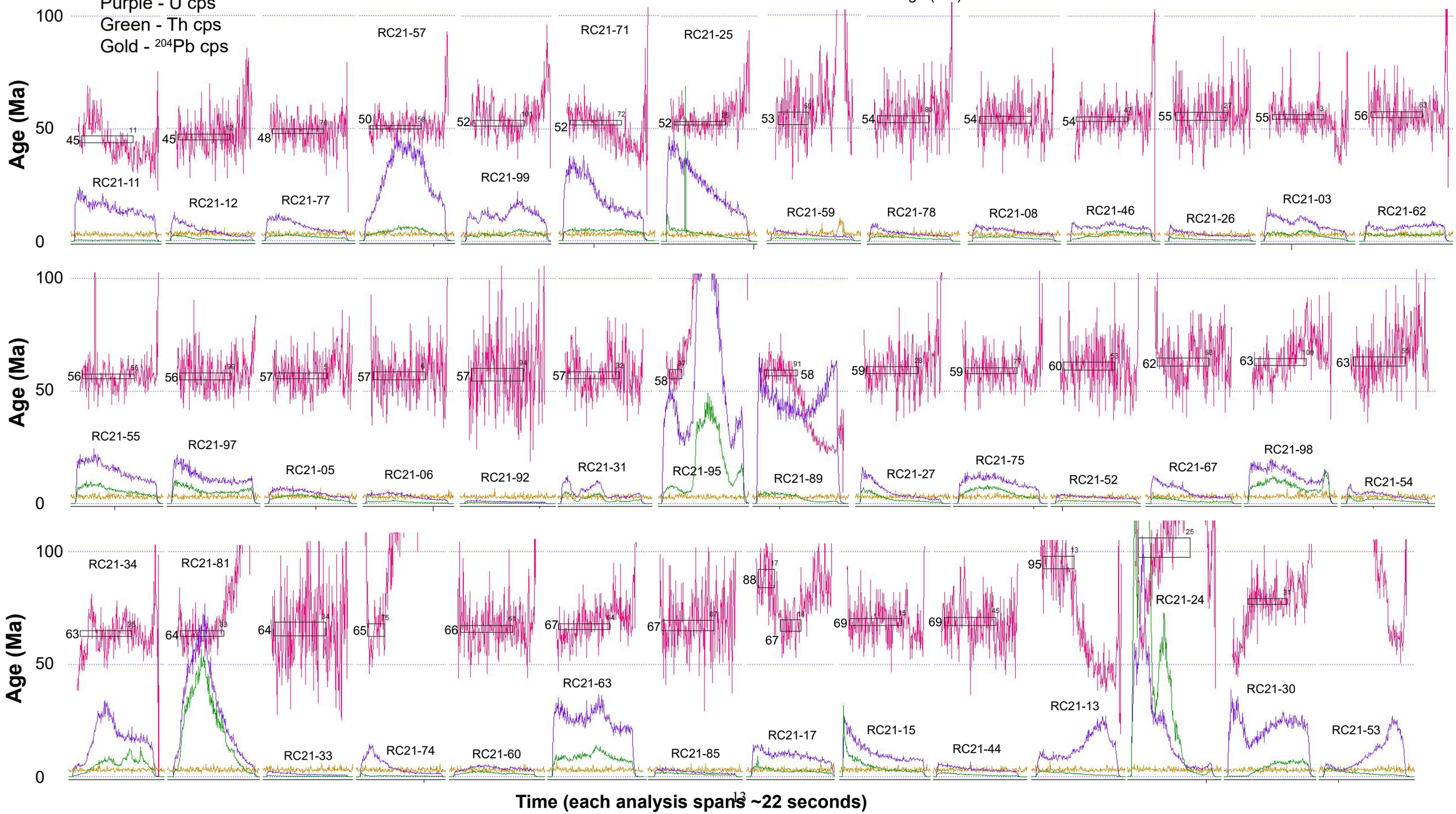
RC21
Red - 6/8 age
Purple - U cps
Green - Th cps
Gold - 204Pb cps
Small numbers to upper right of integration boxes indicate integration number
Larger numbers generally to the left of the integration box indicate age in Ma (207 corrected)
Traces for 6/8 age (red) are not corrected for common lead
Age (Ma)
100
50
0
RC21-11
RC21-12
RC21-77
RC21-57
RC21-99
RC21-71
RC21-25
RC21-59
RC21-78
RC21-08
RC21-46
RC21-26
RC21-03
RC21-62
RC21-55
RC21-97
RC21-05
RC21-06
RC21-92
RC21-31
RC21-95
RC21-89
RC21-27
RC21-75
RC21-52
RC21-67
RC21-98
RC21-54
RC21-34
RC21-81
RC21-33
RC21-74
RC21-60
RC21-63
RC21-85
RC21-17
RC21-15
RC21-44
RC21-13
RC21-24
RC21-30
RC21-53
Time (each analysis spans ~22 seconds)

Figure DR3. Cathodoluminescence images of selected Cemetery Ridge metasandstone zircon mounts (6 pages of graphs).

During LA-ICP-MS analysis, positions for laser spots were selected randomly without prior cathodoluminescence (CL) imaging. This approach has worked well for our studies of other bodies of PORS and for Upper Cretaceous to Eocene sedimentary units of the southern California forearc basin, for which relatively few analyses show evidence of age zonation (Grove et al., 2003; Jacobson et al., 2011). However, after the complexity of the LA-ICP-MS results from Cemetery Ridge became evident, we obtained CL images for six of the eight metasandstone samples (CR33, CR34, CR65, RC13A, RC18, and RC21). The images reveal various complexities in the zonation patterns. Particularly common is a thin outer bright rim followed by a thicker dark inner rim. We attribute the bulk of the various rim and truncation features to Paleogene metamorphism. Future LA-ICP-MS analyses are planned for which spot choice will be guided by the CL imagery.

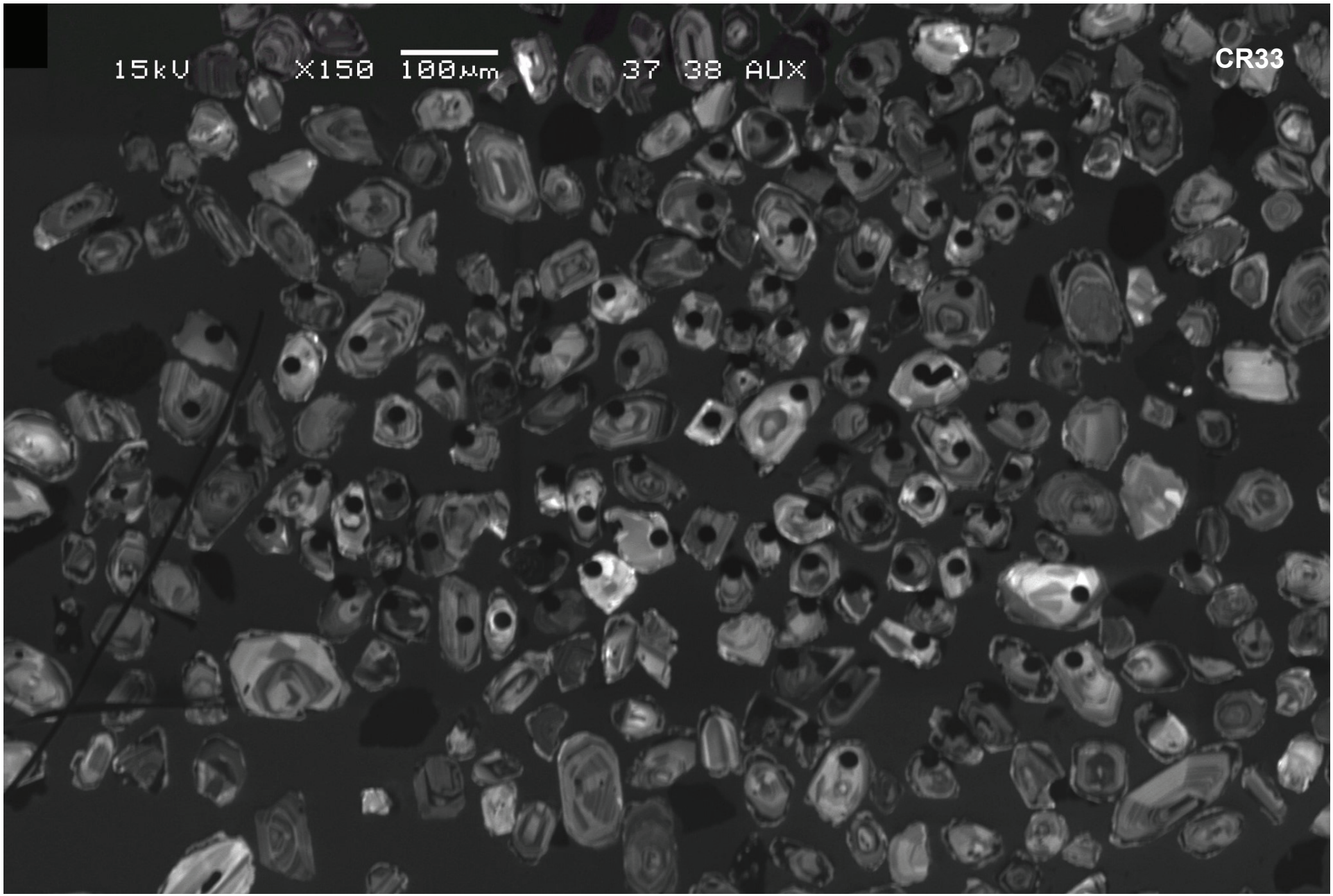
15kV X150 100µm 37 38 AUX
CR33

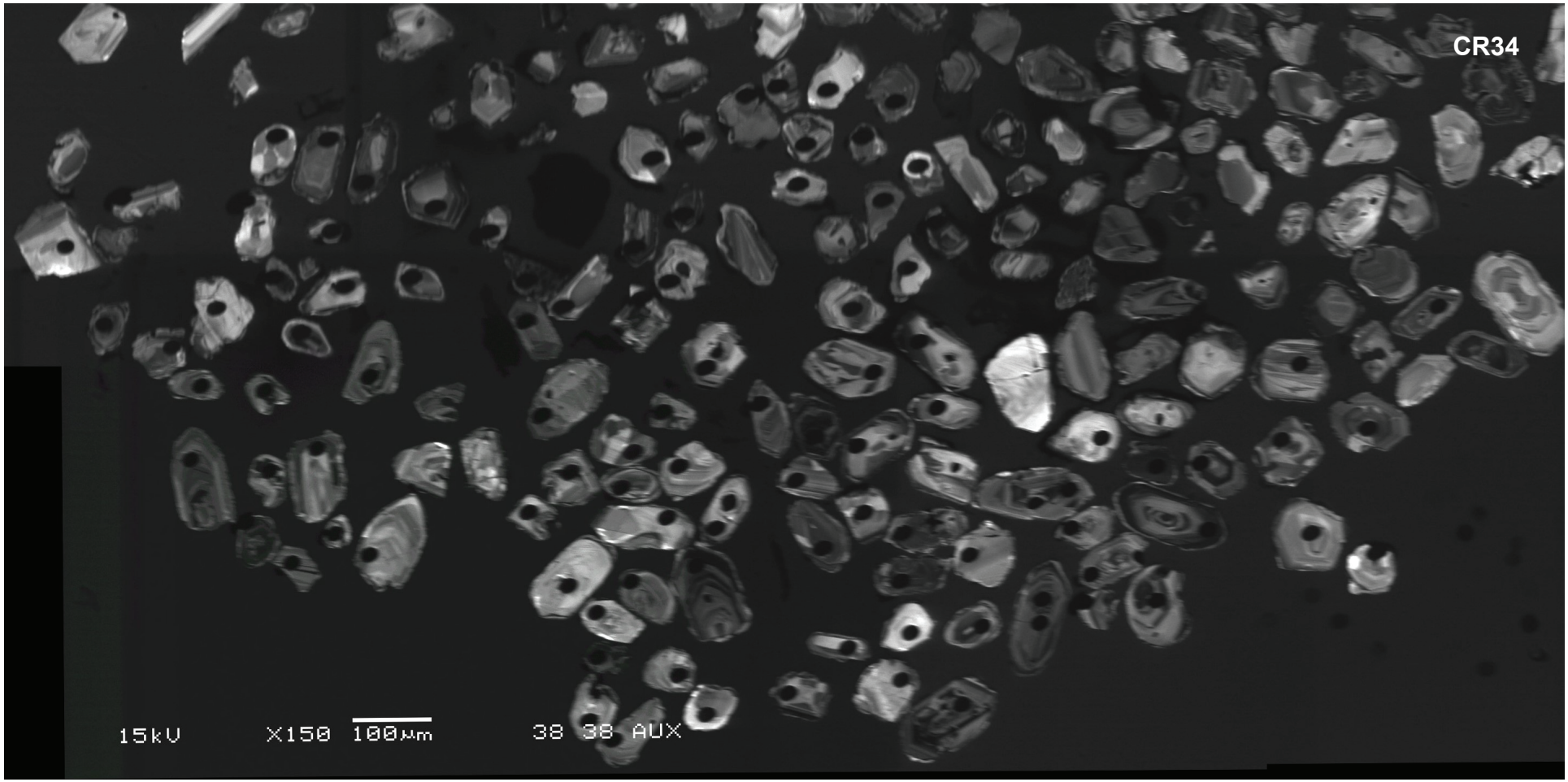
CR34
15kV
X150
100µm
38 38 AUX

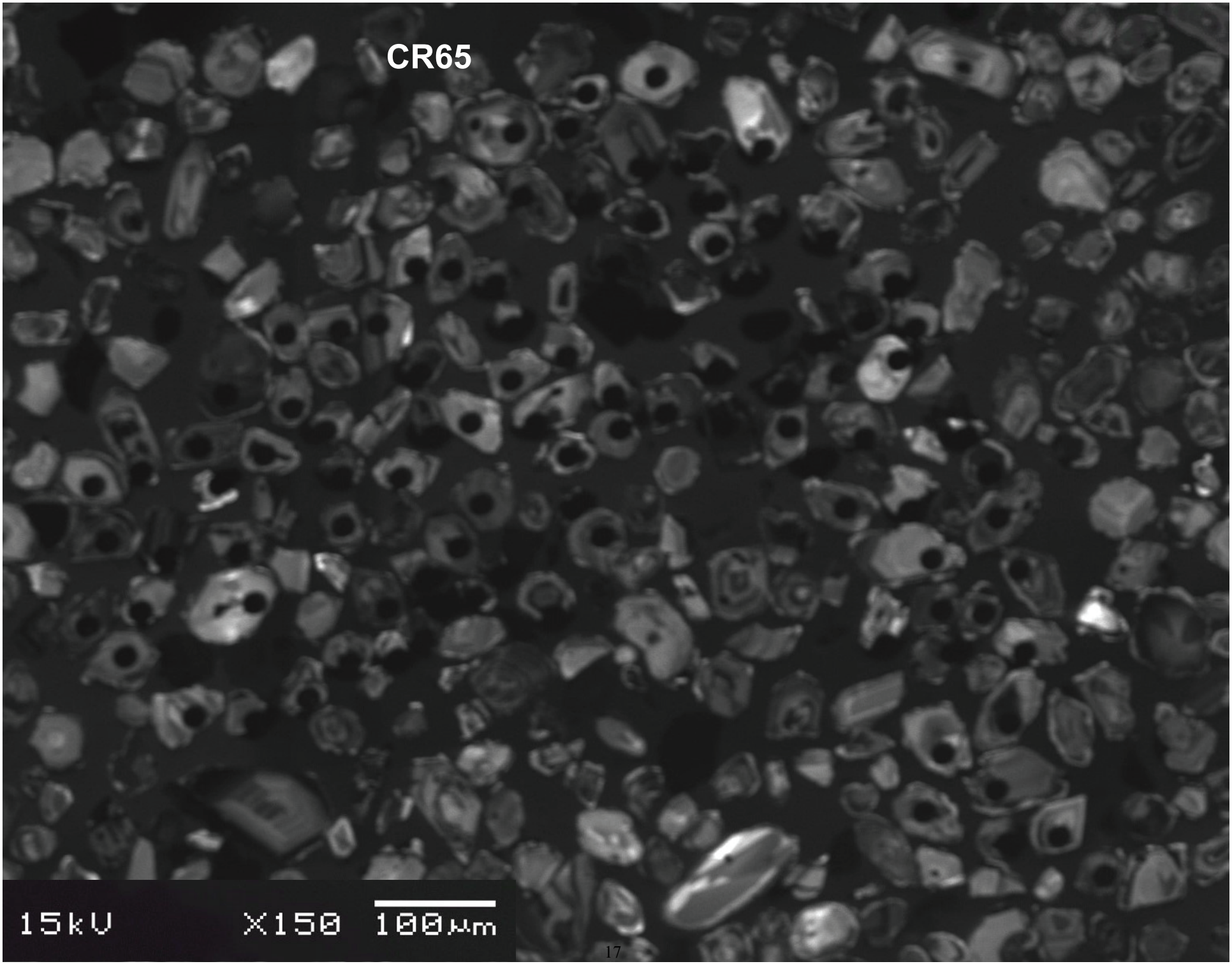
CR65
15kV
X150
100µm

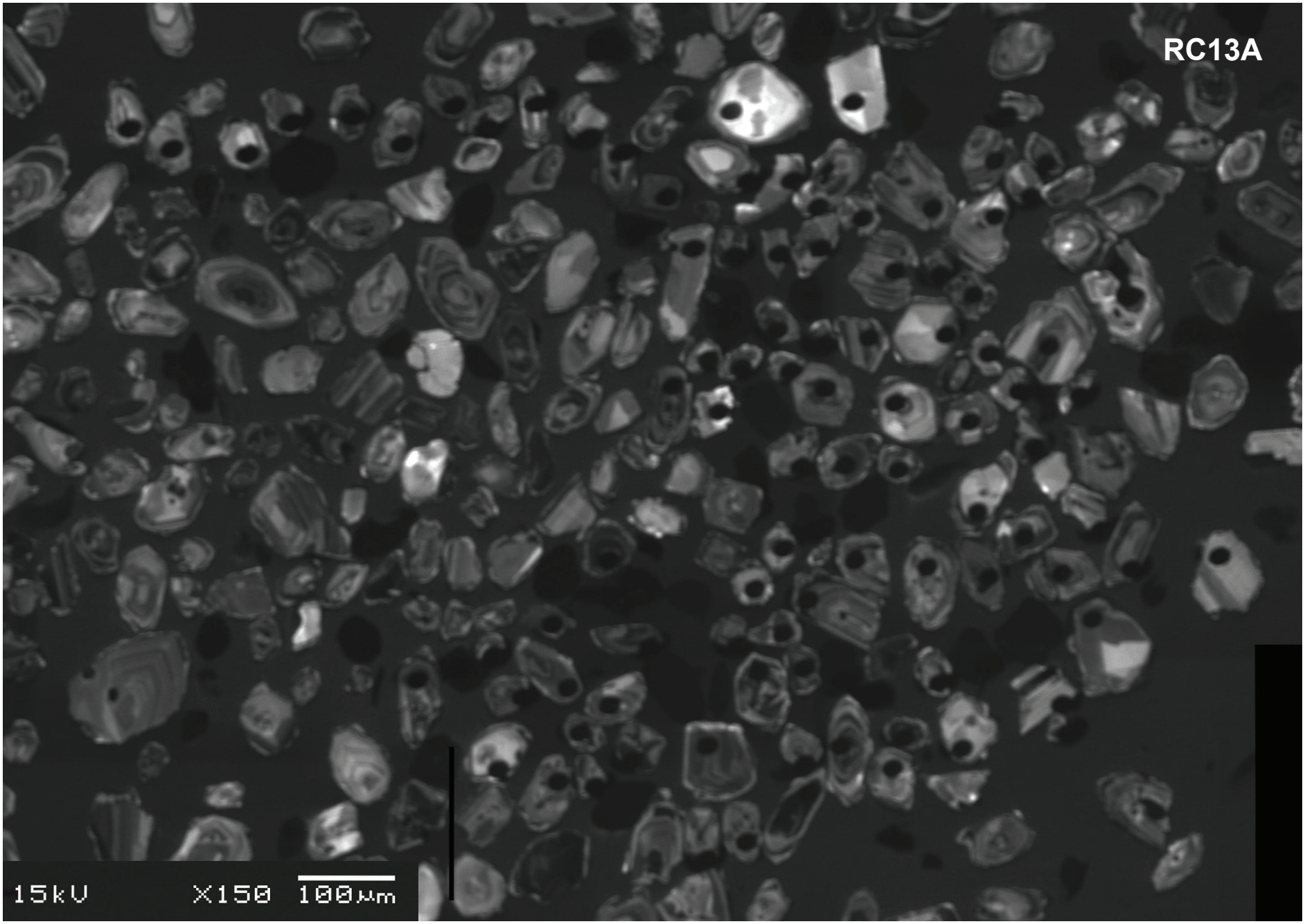
RC13A
15kV
X150
100µm

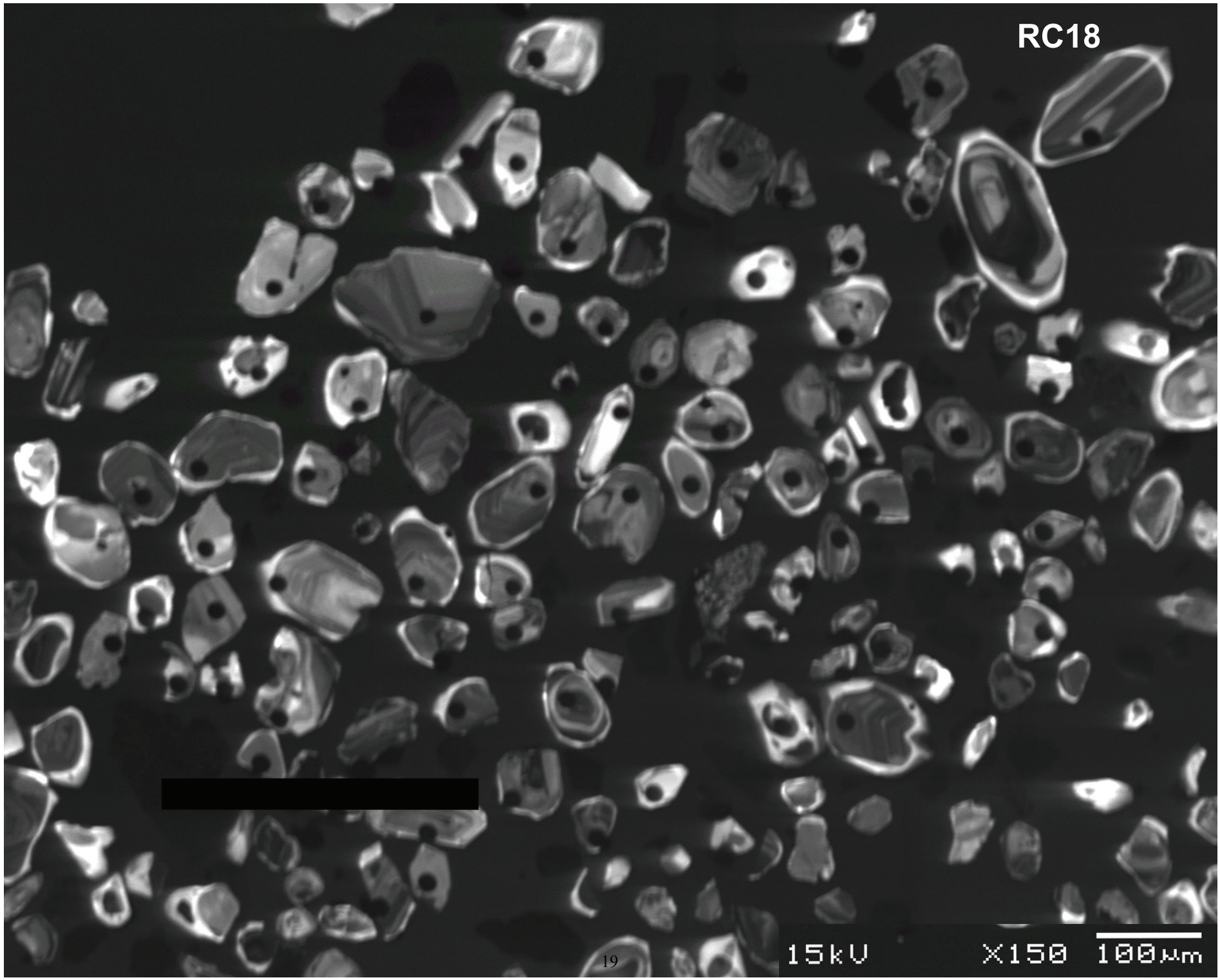
RC18
15kV
X150
100µm

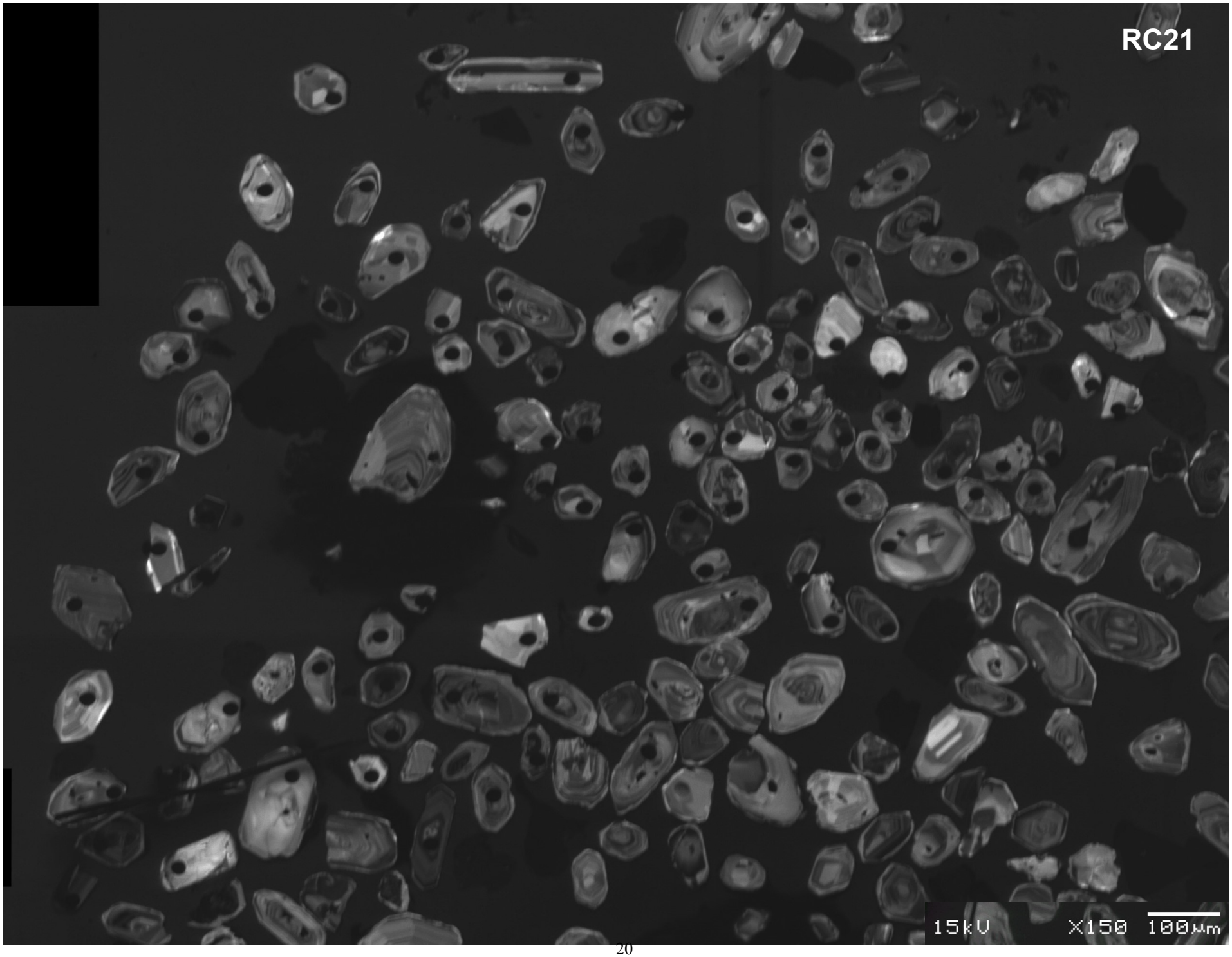
RC21
15kV X150 100µm

Figure DR4. Plots of Th/U and U/Th versus $^{206}Pb/^{238}U$ age for Cemetery Ridge metasandstone zircons with ages < 200 Ma (2 pages of graphs).

The first page of graphs shows U/Th versus age. The second page presents exactly the same data, but in this case in the form of Th/U versus age. The upper graph on each page uses a logarithmic scale for the vertical axis, whereas the lower graph utilizes a linear scale. The logarithmic plots include some analyses that fall outside the range of the linear plots.

Inferred metamorphic zircon (Paleogene ages) exhibit somewhat lower Th/U (higher U/Th) than inferred detrital zircon (Cretaceous and older ages), but the difference is not great.

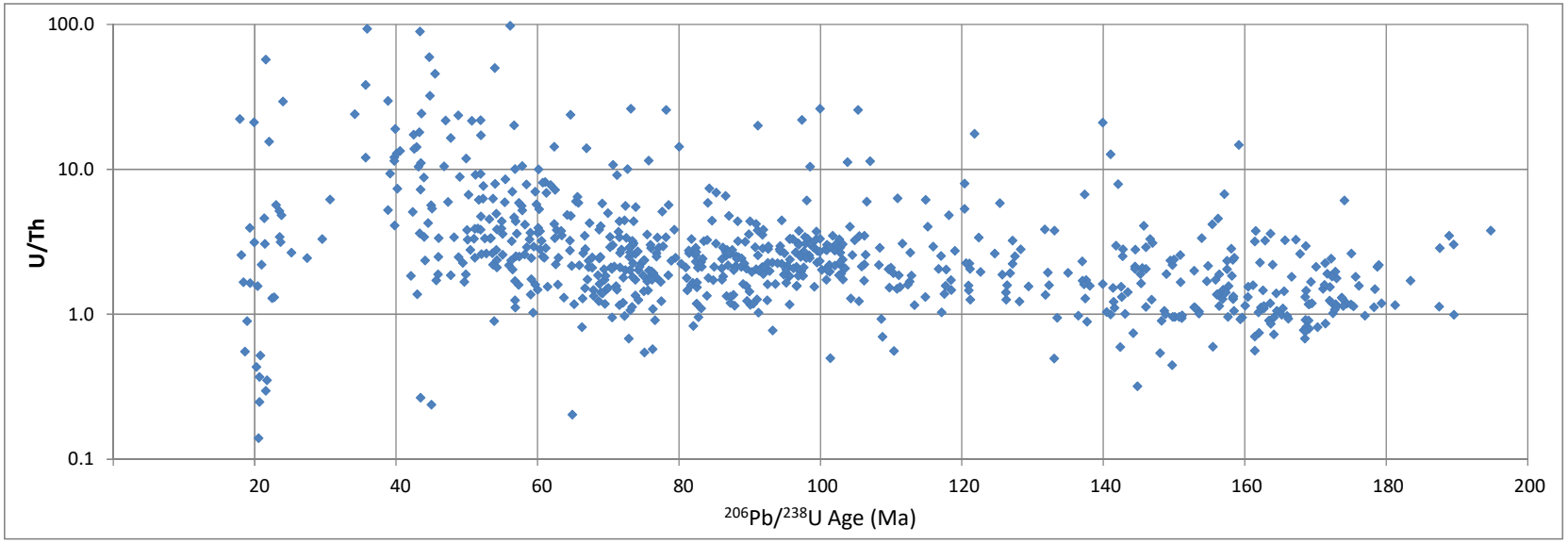
100.0
10.0
1.0
0.1
U/Th
20
40
60
80
100
120
140
160
180
200
206Pb/238U Age (Ma)

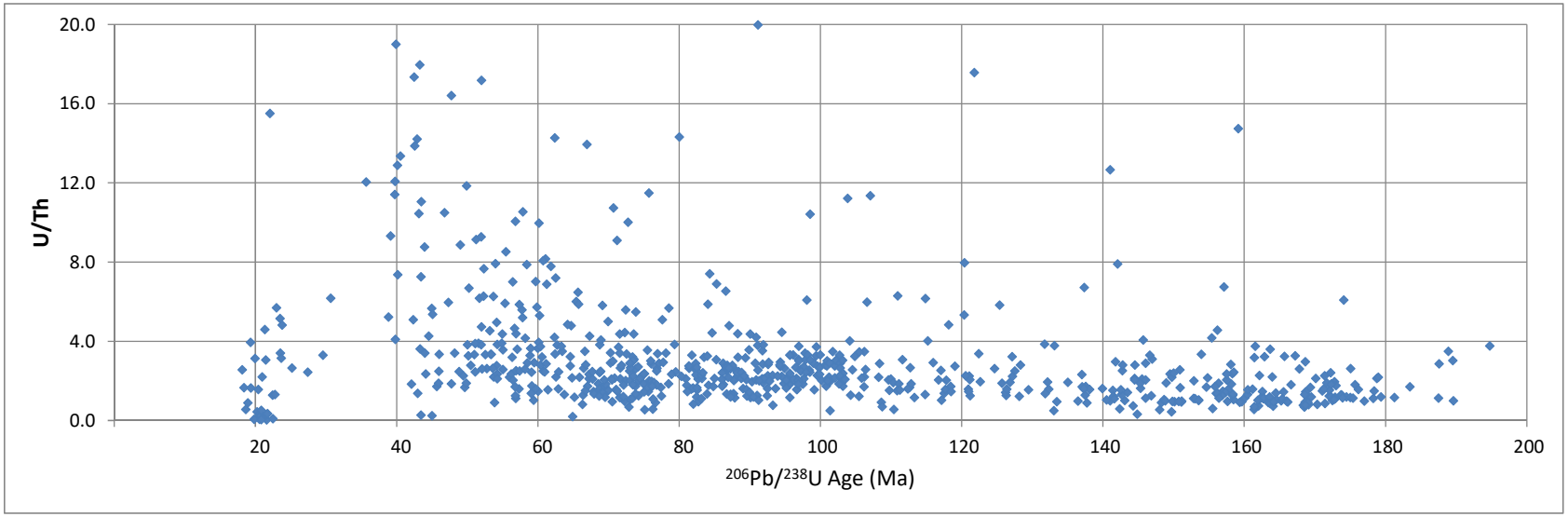
20.0
16.0
12.0
8.0
4.0
0.0
U/Th
20
40
60
80
100
120
140
160
180
200
206Pb/238U Age (Ma)

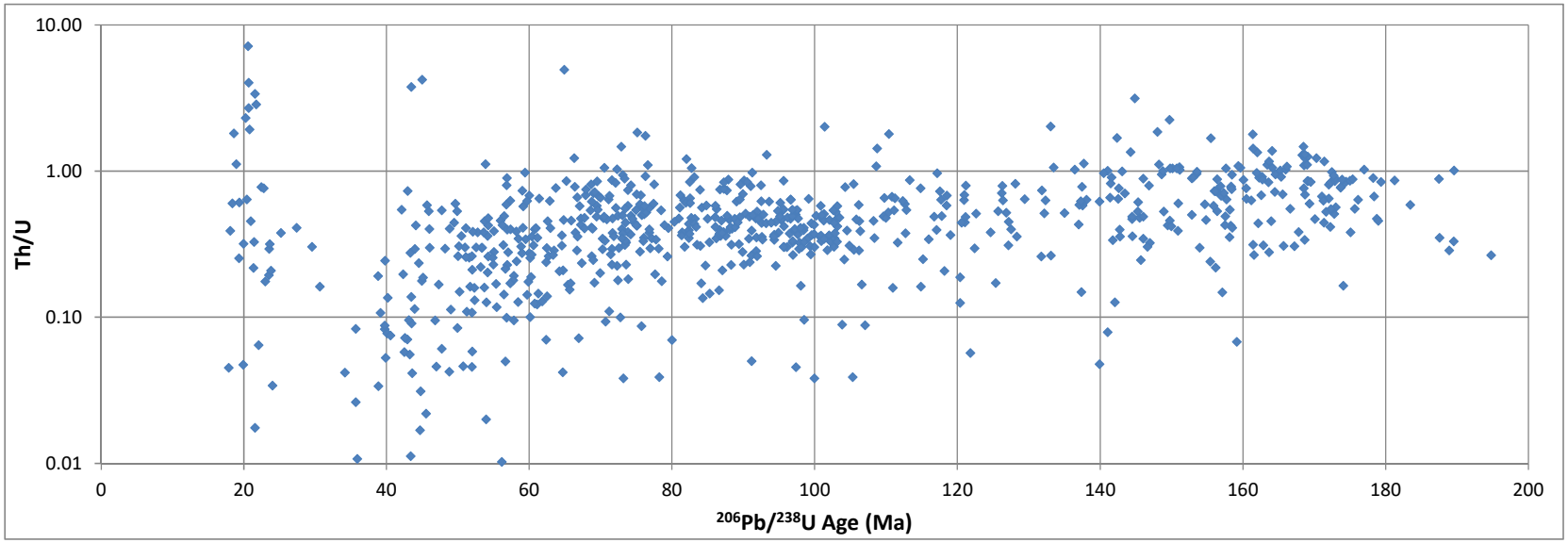
10.00
1.00
0.10
0.01
Th/U
0
20
40
60
80
100
120
140
160
180
200
206Pb/238U Age (Ma)

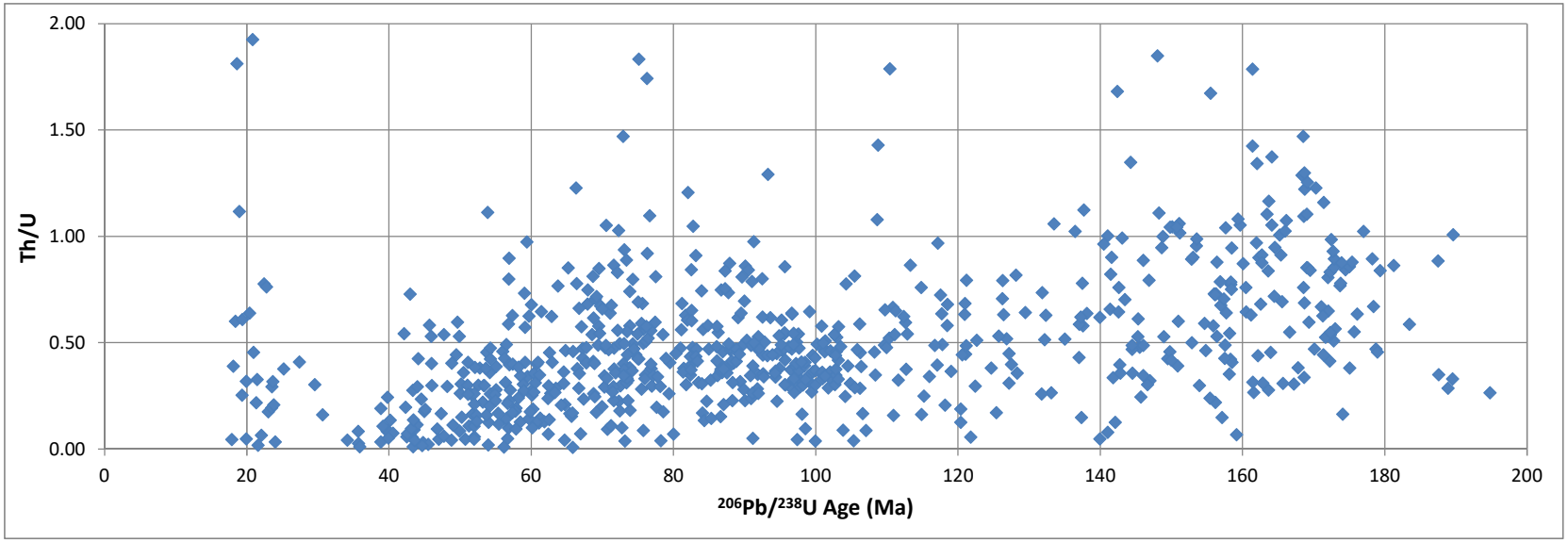
2.00
1.50
1.00
0.50
0.00
Th/U
0
20
40
60
80
100
120
140
160
180
200
206Pb/238U Age (Ma)

Figure DR5. Concordia diagrams of zircon results for individual Orocopia Schist metasandstone samples from Cemetery Ridge (6 pages of graphs).

Diagrams created using Isoplot 3.75 (Ludwig, 2012). Ellipses represent 2σ propagated errors (Appendix DR1). Analyses are not corrected for common Pb.

Diagrams are divided into three sets (two pages each) successively showing (a) conventional (Wetherill) concordia diagrams scaled to include ages up to ca. 2000 Ma, (b) conventional concordia diagrams scaled to include ages up to ca. 300 Ma, and (c) inverse (Tera-Wasserburg) concordia diagrams scaled to show all analyses. For all three sets of diagrams, the more northerly samples are shown on the first page, with the more southerly samples on the second page (see Fig. 1B of the main manuscript for sample locations).

All analyses that fall within the scale range of each diagrams are included, except those deemed not to be zircon. Ellipses in all diagrams represent 2σ propagated errors (Appendix DR1).

The plots reveal two types of discordance. In one case, discordant analyses define chords that project from plausible Proterozoic ages (mostly ca. 1700–1400 Ma; Grove et al., 2003; Jacobson et al., 2011) toward the vicinity of the origin. We interpret this form of discordance as largely the result of Pb loss during Paleogene metamorphism and growth of new zircon (see main text), although inheritance could also play a role. This type of discordance is most evident in the conventional concordia diagrams that include ages up to ca. 2000 Ma. All eight metasandstone samples exhibit this style of discordance. In general, the degree of discordance is much greater for Cemetery Ridge samples than for the PORS elsewhere or for unmetamorphosed Upper Cretaceous–Paleogene sedimentary sequences in southern California that were derived from the same source areas as the PORS (Grove et al., 2003; Jacobson et al., 2011). We attribute the apparent lead loss to the relatively high temperature of metamorphism at Cemetery Ridge.

A second type of discordance relates to the presence of common Pb. This type of discordance is indicated in the conventional concordia diagrams by analyses that lie off concordia along arrays that slope gently to the upper right. These arrays project to upper-intercept ages that are unrealistically old for the PORS, and in many cases older than the age of Earth. In the inverse concordia diagrams, this type of discordance is indicated by arrays that project toward $^{207}Pb/^{206}Pb \approx 0.8$. As with the conventional concordia diagrams, the upper intercepts imply unrealistically old ages, but are consistent with isotopic composition of common Pb. Discordance due to common Pb is particularly clear for sample RC18, which includes a large population of discordant early Miocene grains. Equally well-defined arrays confirming the presence of common Pb are also evident in several of the early Miocene intrusive rocks (below). The effect of common Pb is greatest for zircon with low radiogenic Pb; i.e., young zircon or zircon with low U. All samples include at least some grains that appear to be discordant owing to the presence of common Pb. The effect is greatest in samples CR65, RC9, CR33, RC13A, and RC18. We are not sure whether the common Pb is geological in origin or was introduced during sample preparation and/or analysis.

Because any individual grain can be discordant owing to lead loss and/or common lead contamination, interpreting the ages of discordant grains is problematic. As described in

Appendix DR1, we are unable to use ^{204}Pb to correct for common Pb. To minimize the impact of common Pb, we excluded analyses or parts of analyses with elevated counts for mass 204. We further assumed that Pb loss was the dominant cause of discordance for "old" ages, especially those with $^{206}Pb/^{238}U$ age > 800 Ma, for which we used $^{207}Pb/^{206}Pb$ age as the "best" age. For these results, we excluded analyses with greater than 30% normal discordance or 10% reverse discordance ($^{207}Pb/^{235}U$ versus $^{206}Pb/^{238}U$ age) from probability plots (e.g., Fig. 2 in the main text and Fig. DR1). In contrast, all analyses, irrespective of degree of discordance, are included in the concordia plots (i.e., this figure) to illustrate the situation.

Despite the high degree of discordance, the close correspondence in age of the various Proterozoic populations between the Cemetery Ridge samples and other rocks apparently derived from the same source areas (other Orocopia Schist and lower to middle Eocene forearc units) confirms that neither discordance nor common Pb are a major problem for inferring original crystallization ages for Proterozoic grains at Cemetery Ridge.

The situation, however, is more complicated for analyses with $^{206}Pb/^{238}U$ age < 800 Ma, for which we used the $^{206}Pb/^{238}U$ ages as the best age. The PORS generally includes few ages in the range 800–300 Ma. Hence, most analyses for which the best age is the $^{206}Pb/^{238}U$ age are in a range (i.e., <300 Ma) that could be strongly affected by both Pb loss/inheritance and common Pb. For these analyses, we were forced to use a subjective approach in which we examined the position of each analysis on the conventional and inverse concordia plots to determine degree of concordance/discordance. We eliminated analyses that were offset from discordia by 2-3 times the size of the error ellipse. We viewed this as a compromise between eliminating too many analyses versus including grains that had significant Pb loss/inheritance or required excessive correction for common Pb.

References

Grove, M., Jacobson, C.E., Barth, A.P., and Vućić, A., 2003, Temporal and spatial trends of Late Cretaceous–early Tertiary underplating of Pelona and related schist beneath southern California and southwestern Arizona, *in* Johnson, S.E., Patterson, S.R., Fletcher, J.M., Girty, G.H., Kimbrough, D.L., and Martin-Barajas, A., eds., Tectonic evolution of northwestern Mexico and the southwestern USA: Geological Society of America Special Paper 374, p. 381–406, doi:10.1130/0-8137-2374-4.381.

Jacobson, C.E., Grove, M., Pedrick, J.N., Barth, A.P., Marsaglia, K.M., Gehrels, G.E., and Nourse, J.A., 2011, Late Cretaceous-early Cenozoic tectonic evolution of the southern California margin inferred from provenance of trench and forearc sediments: Geological Society of America Bulletin, v. 123, p. 485–506, doi:10.1130/B30238.1.

Ludwig, K.R., 2012, User's manual for Isoplot 3.75: A Geochronological Toolkit for Microsoft Excel: Berkeley Geochronology Center, Special Publication 5, 75 p.

Data-point error ellipses are 2σ

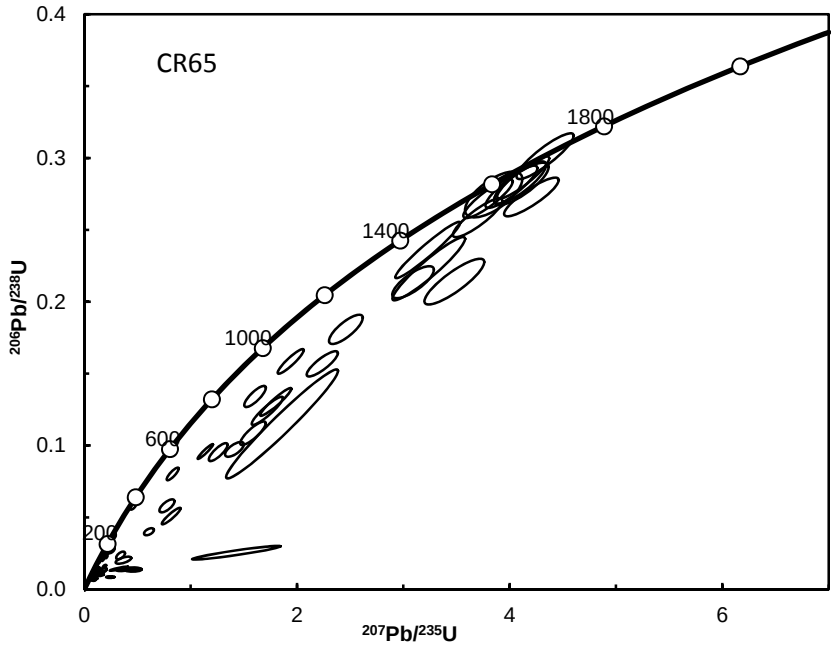

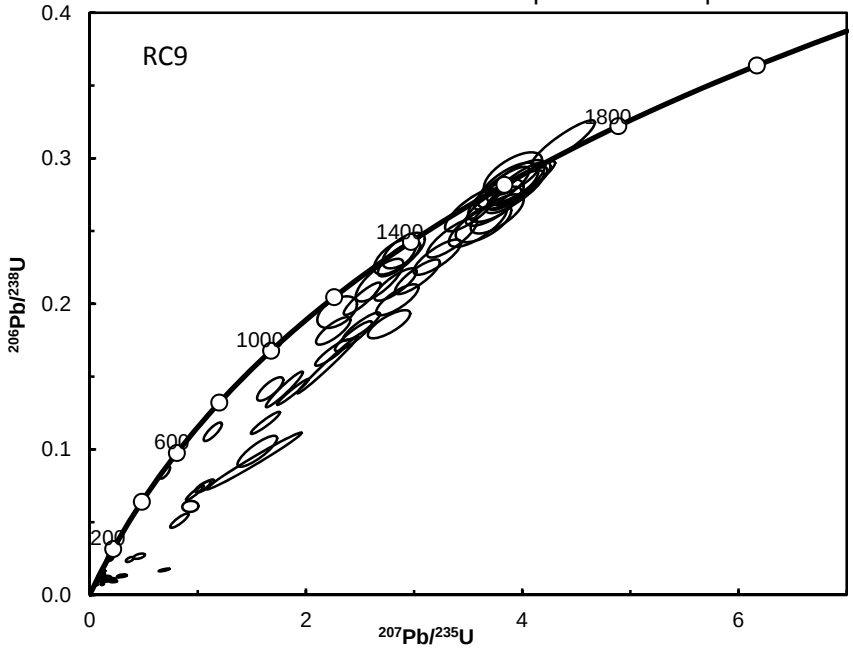

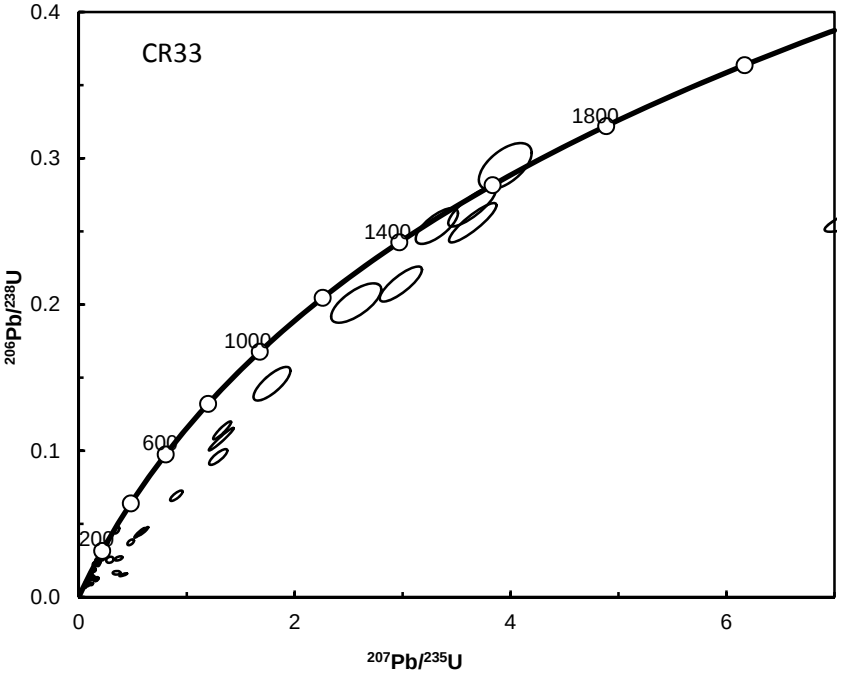

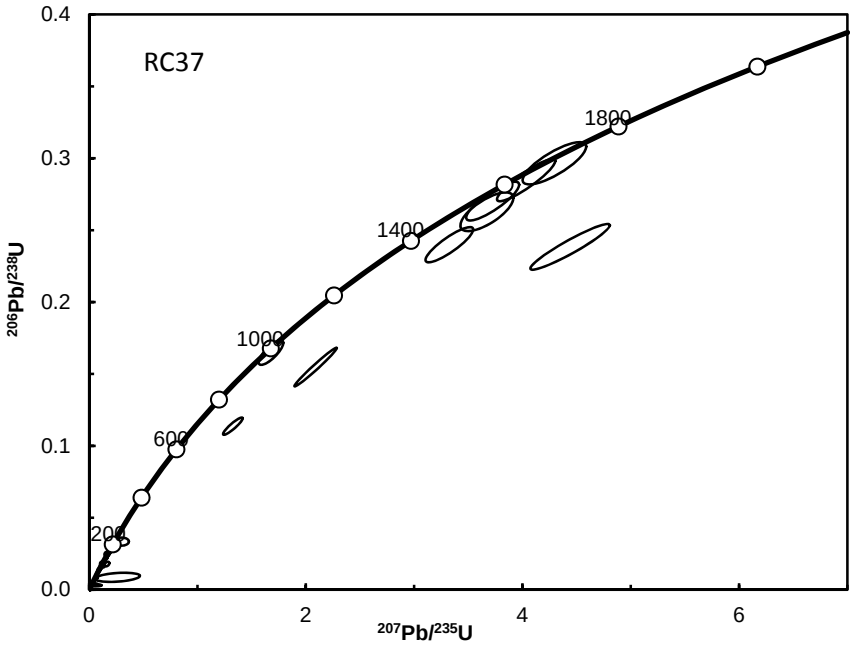

Data-point error ellipses are 2σ

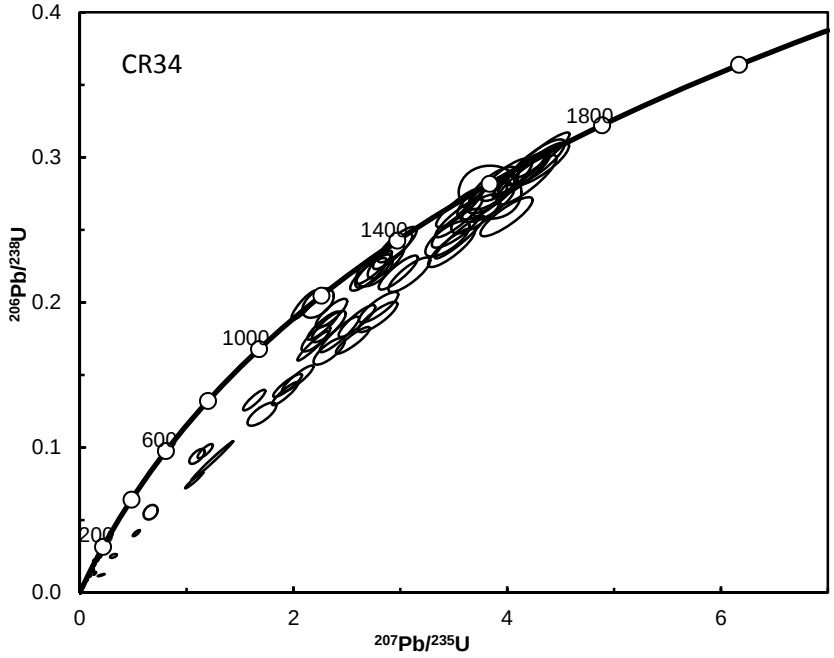

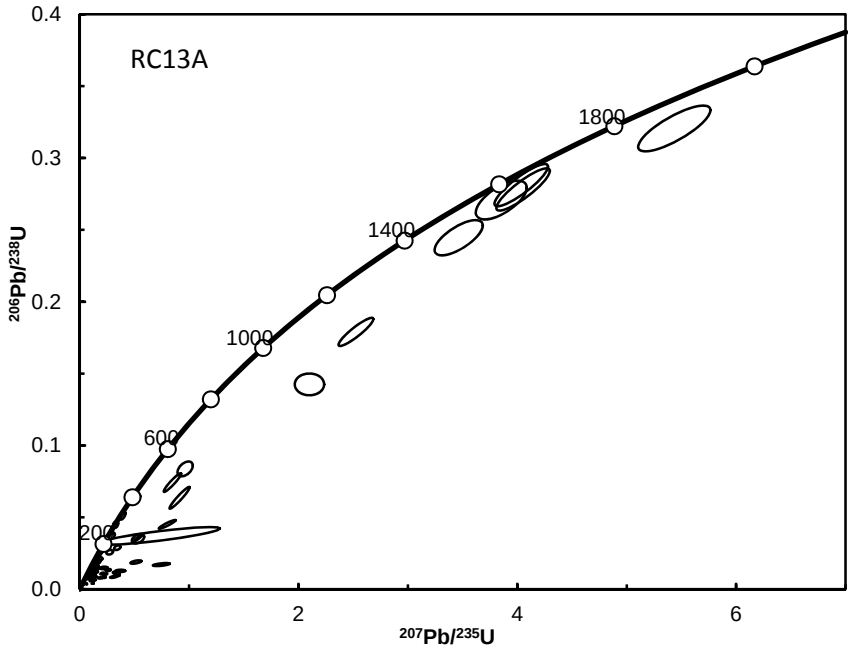

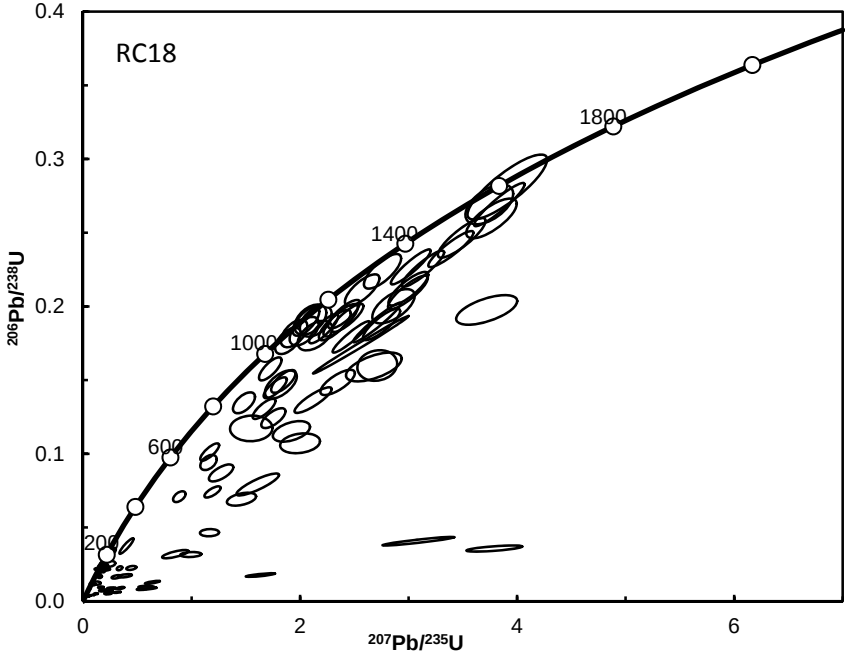

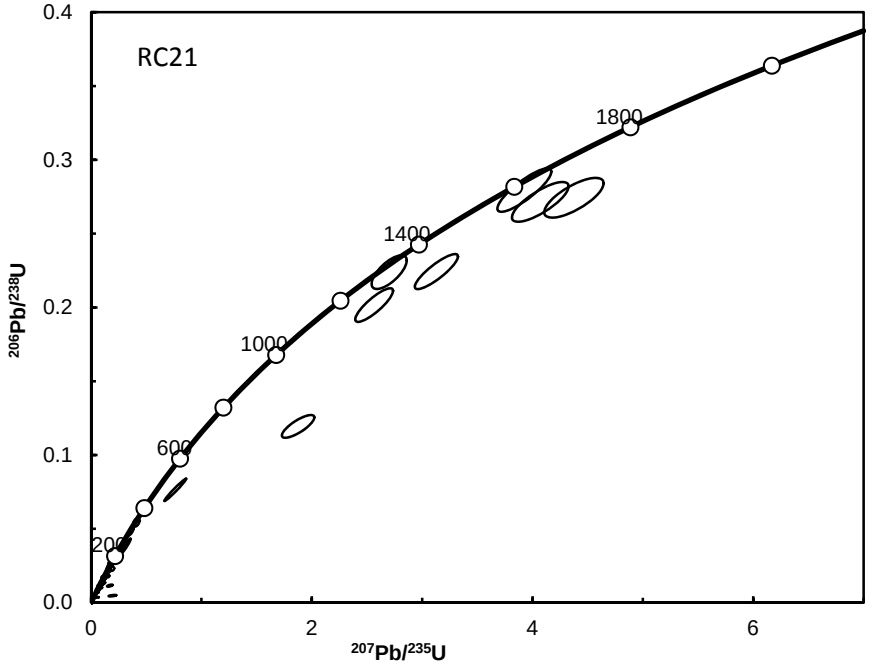

Data-point error ellipses are 2σ

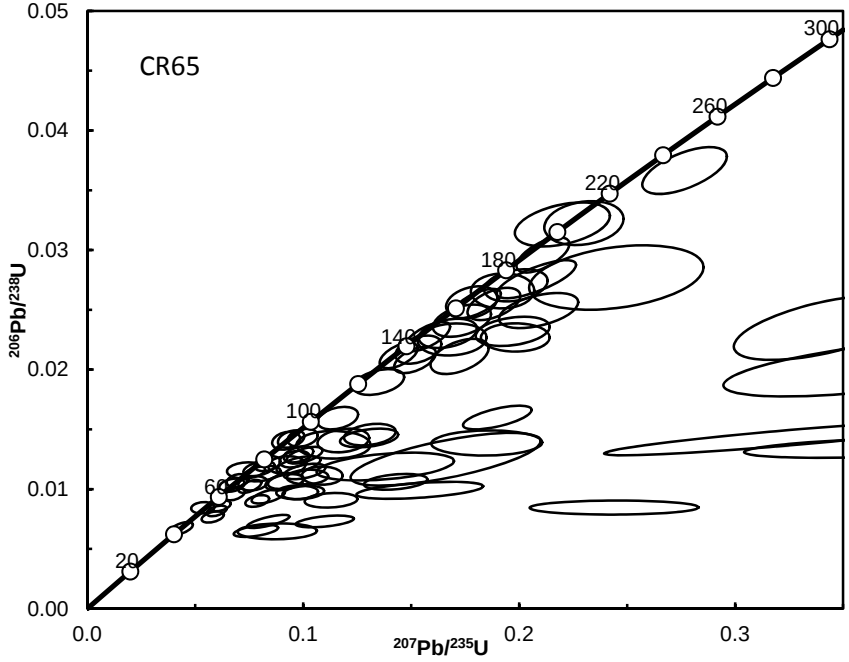

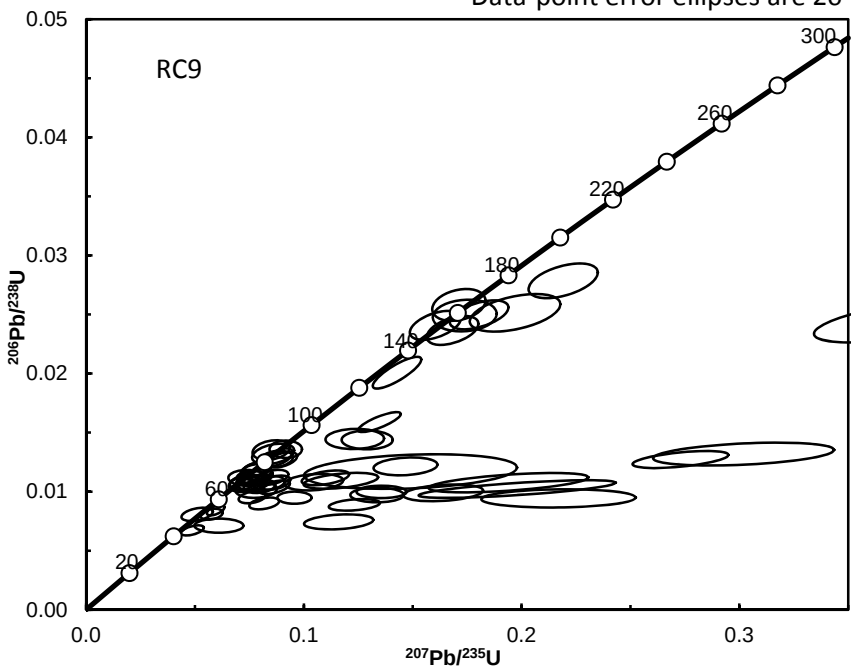

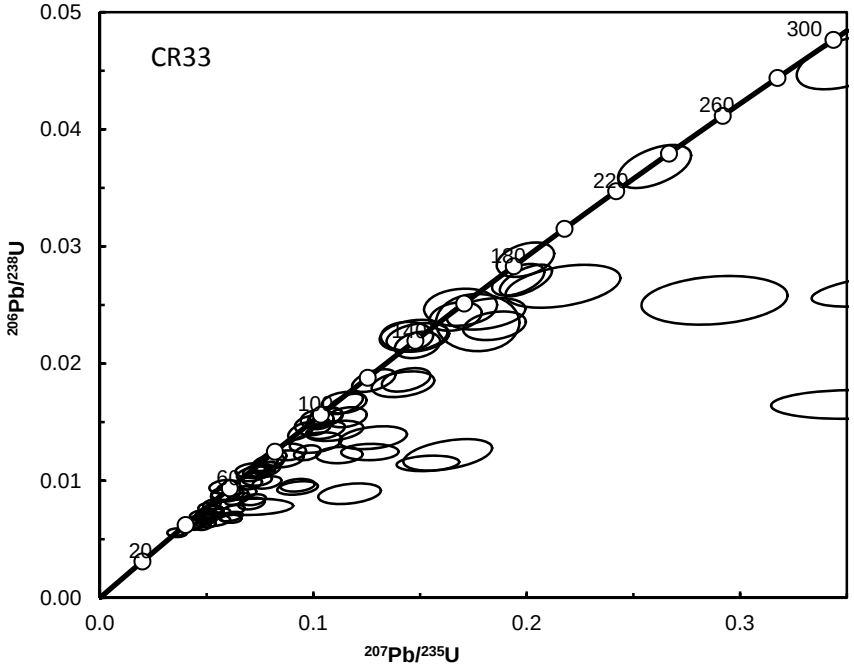

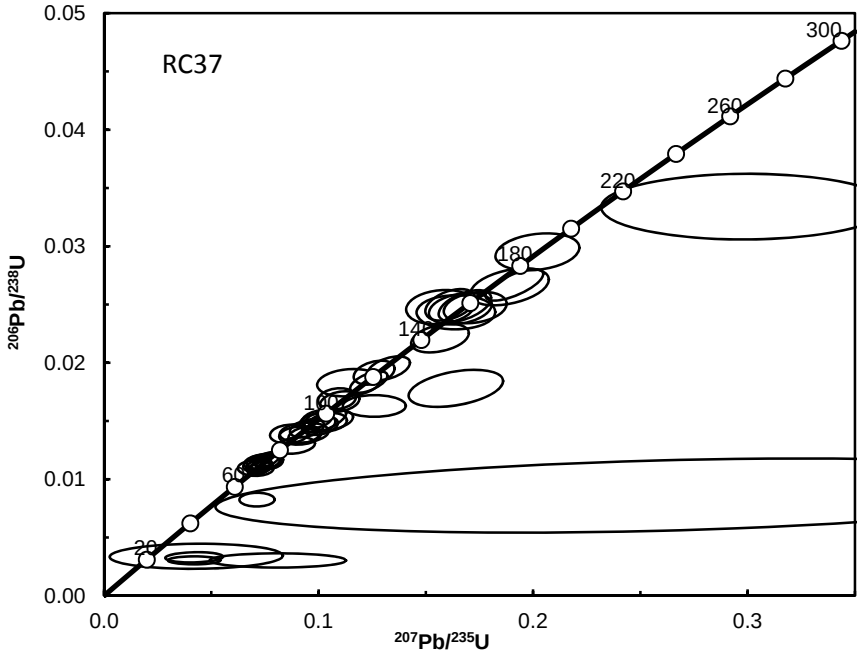

Data-point error ellipses are 2σ

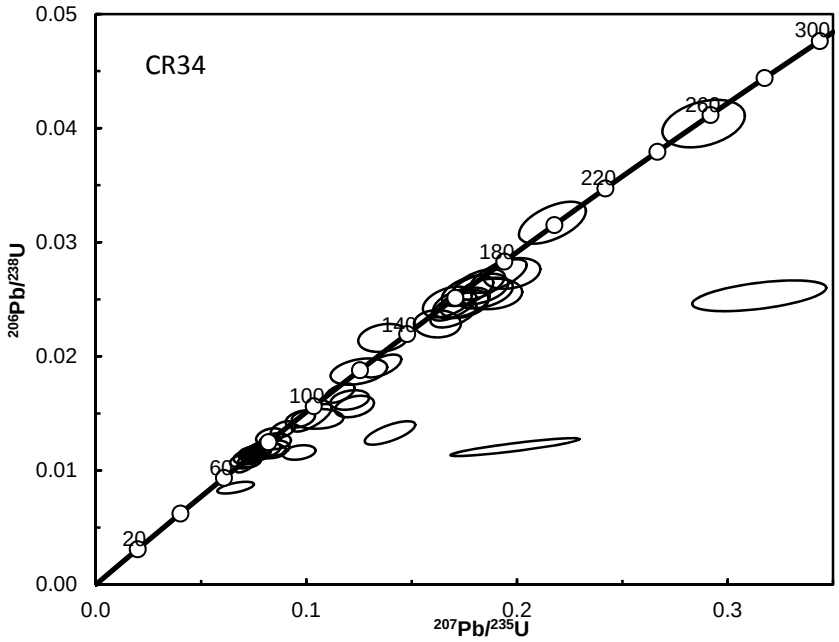

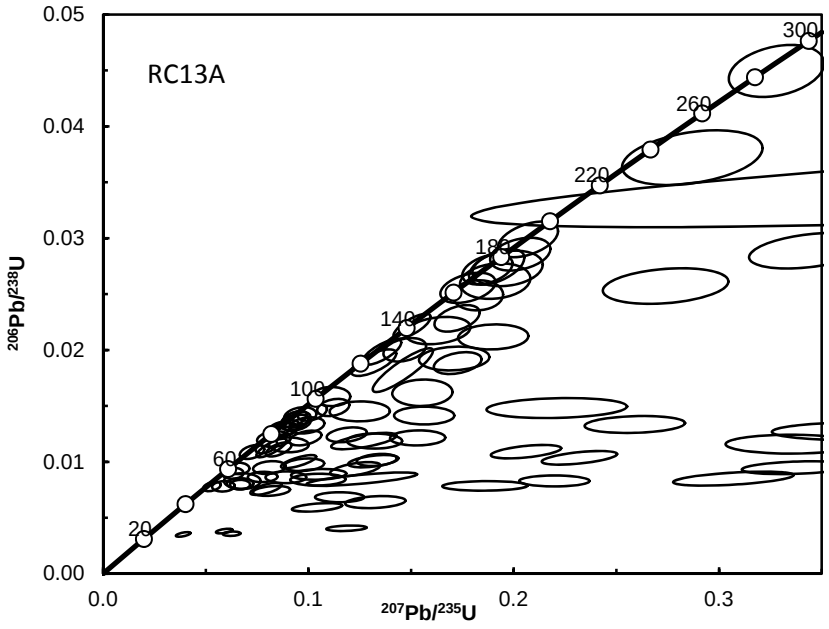

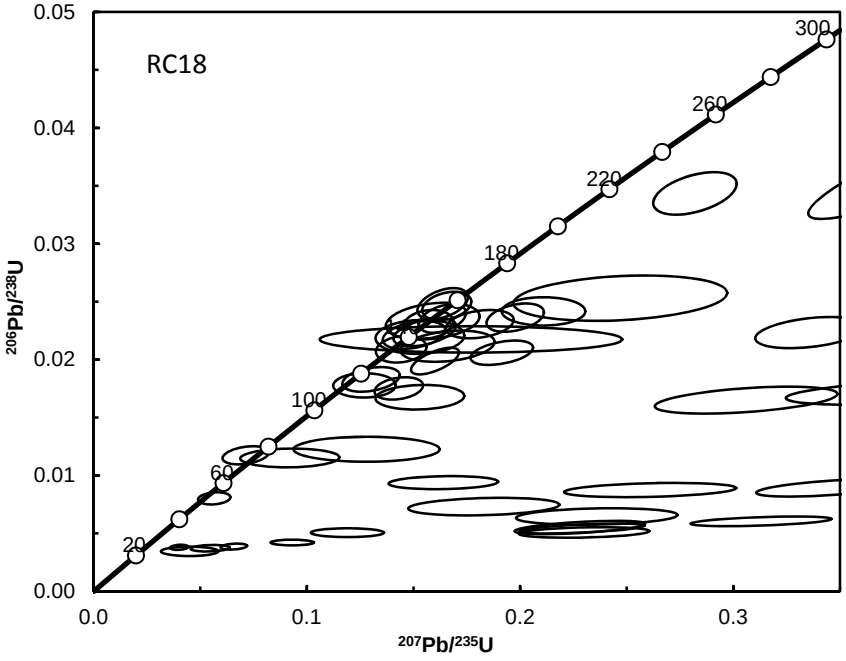

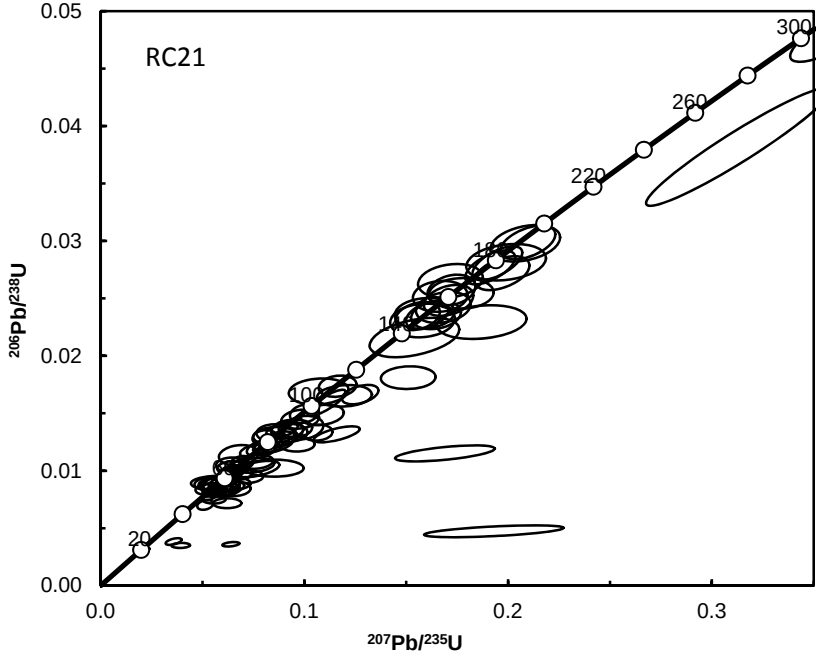

Data-point error ellipses are 2σ

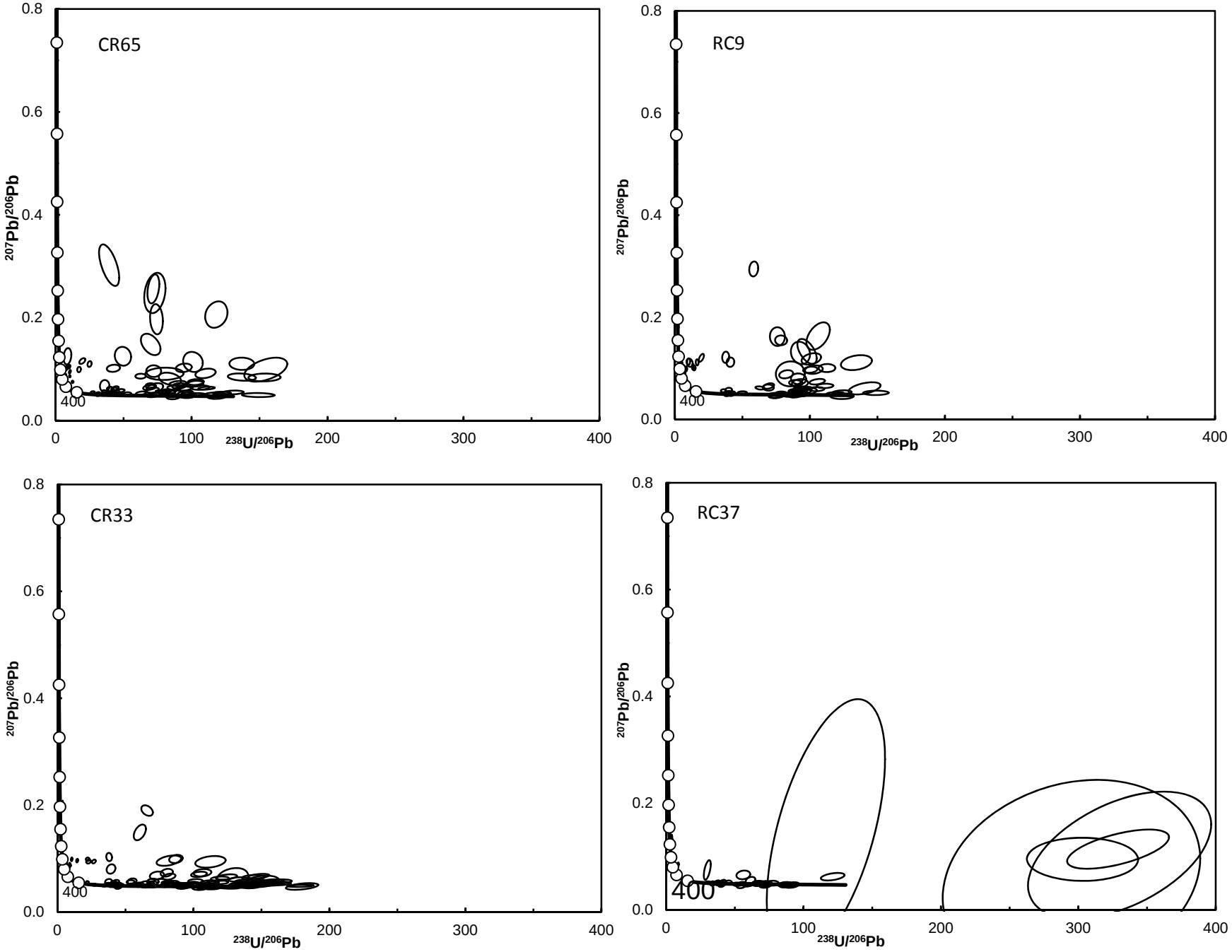

Data-point error ellipses are 2σ

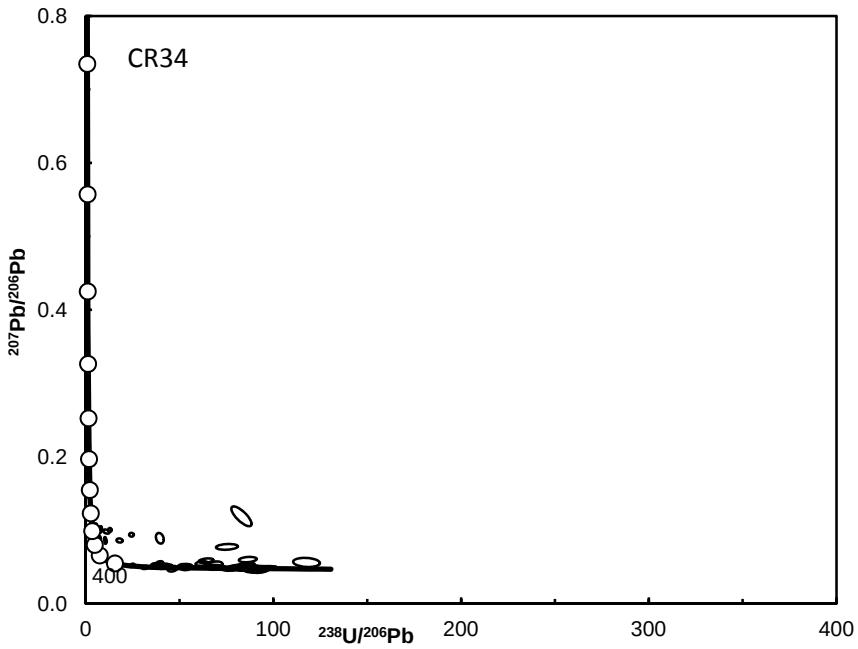

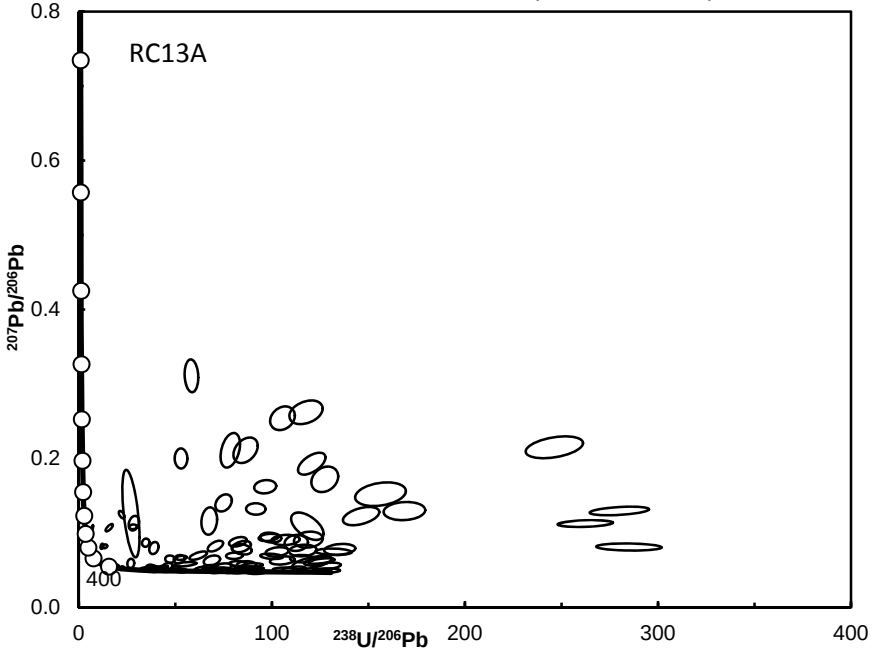

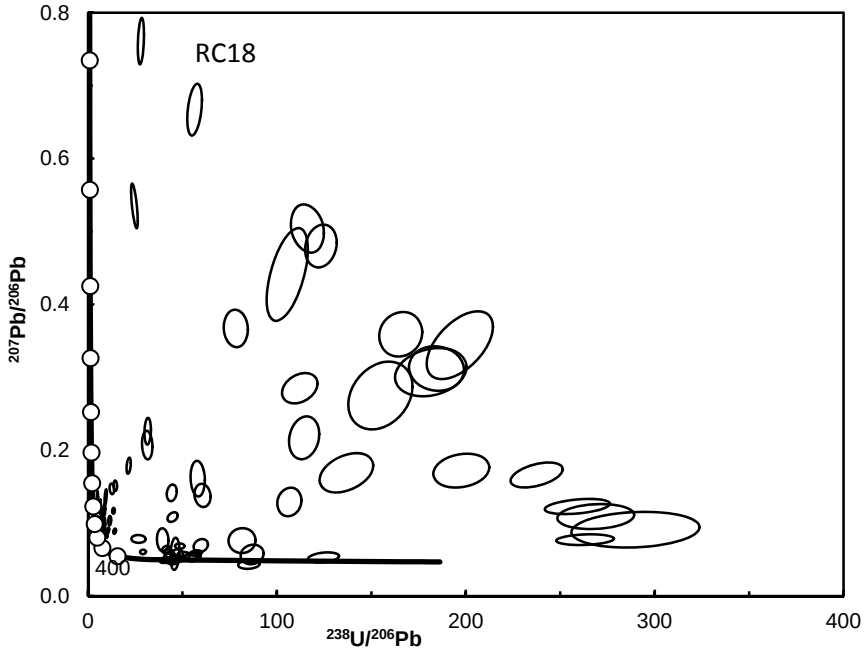

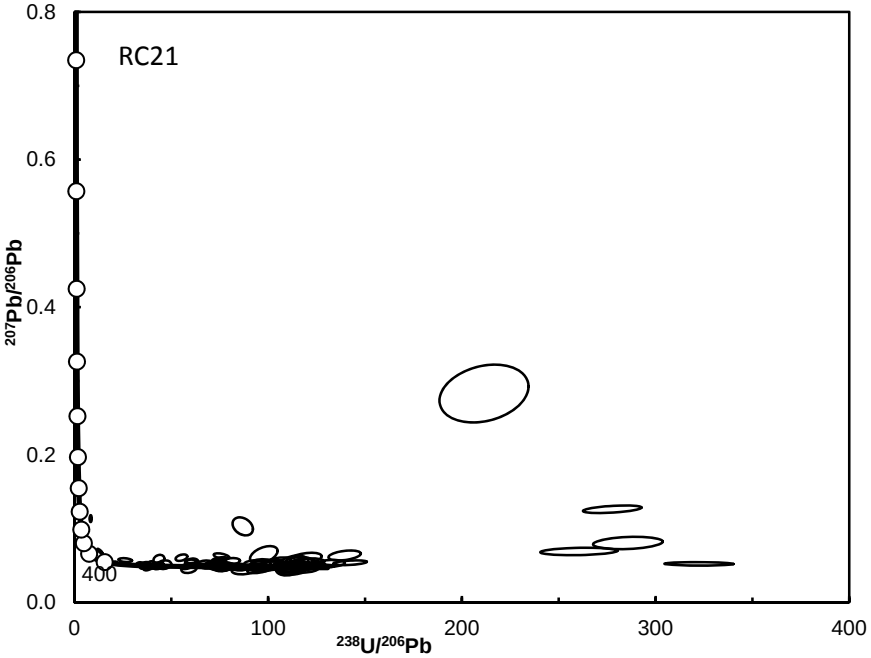

Figure DR6. Concordia diagrams of zircon results for individual igneous samples from Cemetery Ridge (3 pages of graphs).

Diagrams created using Isoplot 3.75 (Ludwig, 2012). Ellipses represent 2σ propagated errors (Appendix DR1). Analyses are not corrected for common Pb.

Inverse (Tera-Wasserburg) concordia diagrams are shown for all eight samples. Conventional (Wetherill) diagrams are included only for samples RC13C and RC47. The latter are the only two samples that yielded inherited grains (16 out of 50 analyses for sample RC13C, 1 out of 22 analyses for sample RC47). See Figure 1B of the main manuscript for sample locations.

For the inverse concordia diagrams, samples are arranged from those with relatively more epizonal textures and less well developed foliation at the top of the first page of the figure to those with relatively more mesozonal textures and more strongly developed foliation at the bottom of the second page. Rock type and degree of fabric development are listed on each diagram. Each diagram also lists the inferred crystallization age and uncertainty (95% confidence interval) based on the weighted mean of the individual analyses (see Fig. DR7).

The inverse concordia diagrams are more complete versions of the graphs included in Figure 3 of the main manuscript. In particular, Figure DR6 includes some discordant analyses excluded from Figure 3 because of space considerations. The discordance is due to contamination with common Pb, similar to that described for the Orocopia Schist metasandstones in Figure DR5.

References

Ludwig, K.R., 2012, User's manual for Isoplot 3.75: A Geochronological Toolkit for Microsoft Excel: Berkeley Geochronology Center, Special Publication 5, 75 p.

Data-point error ellipses are 2σ

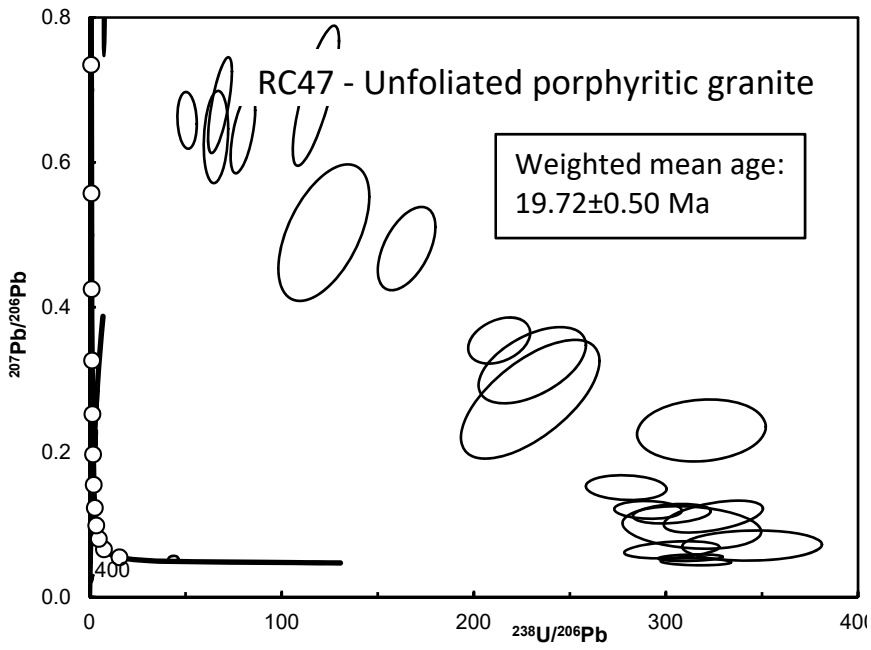

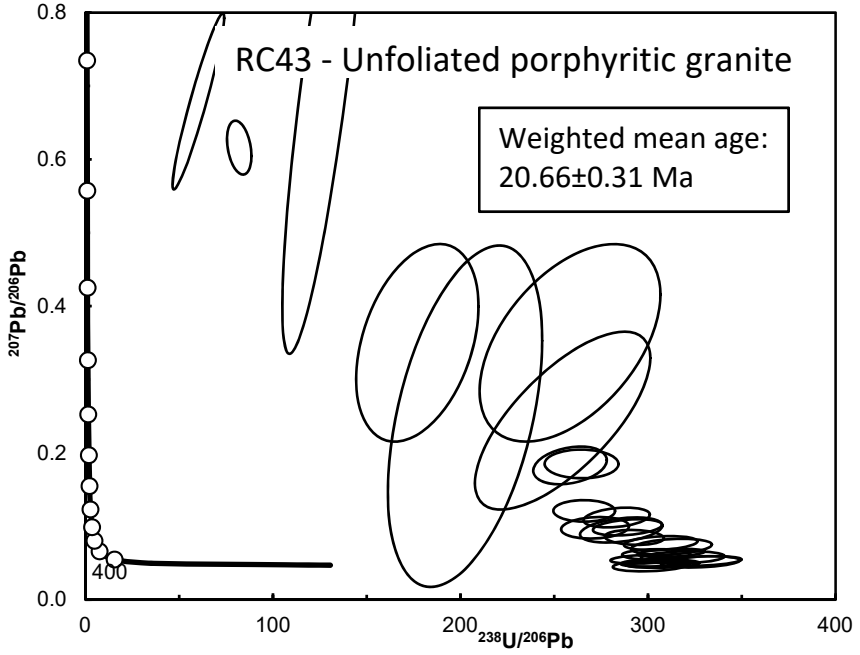

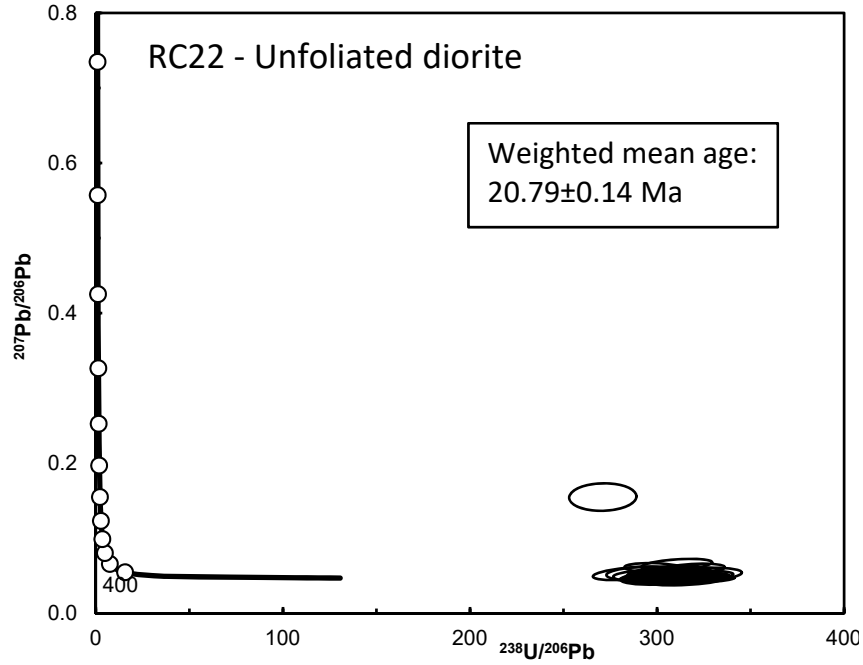

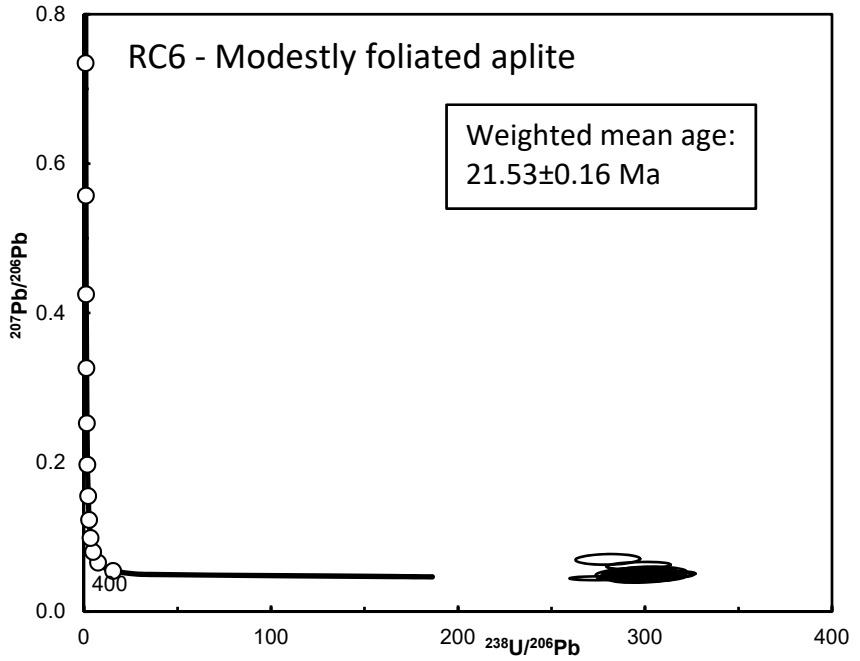

Data-point error ellipses are 2σ

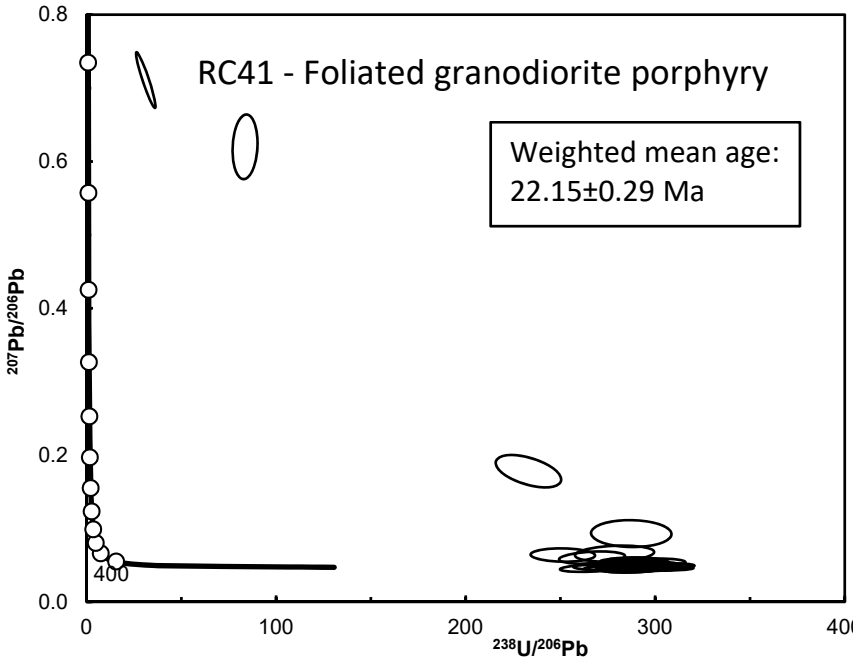

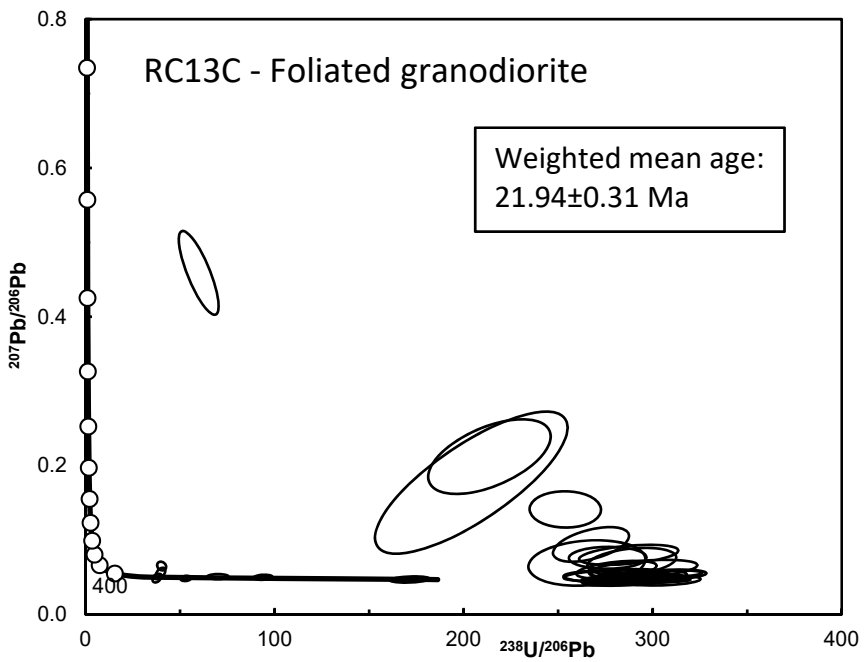

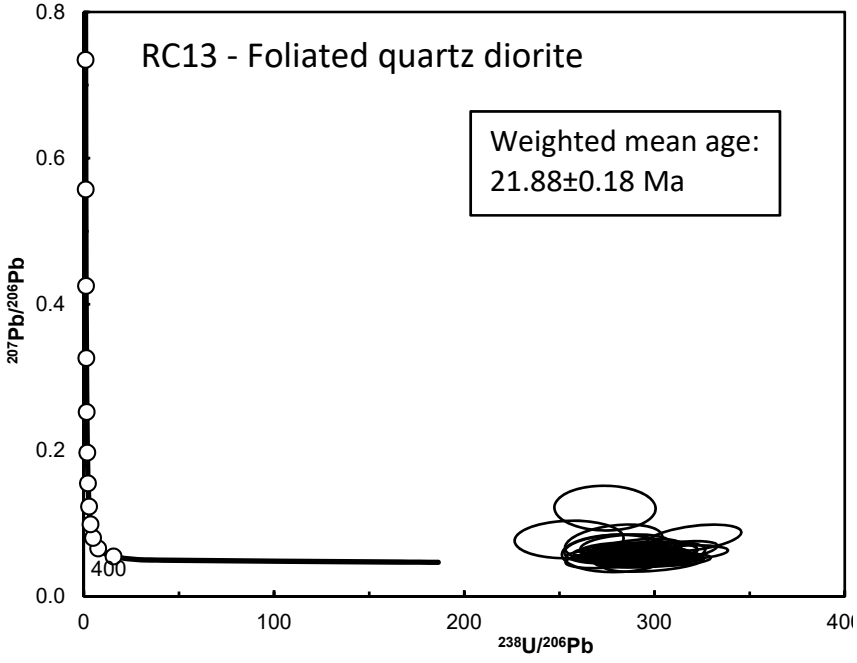

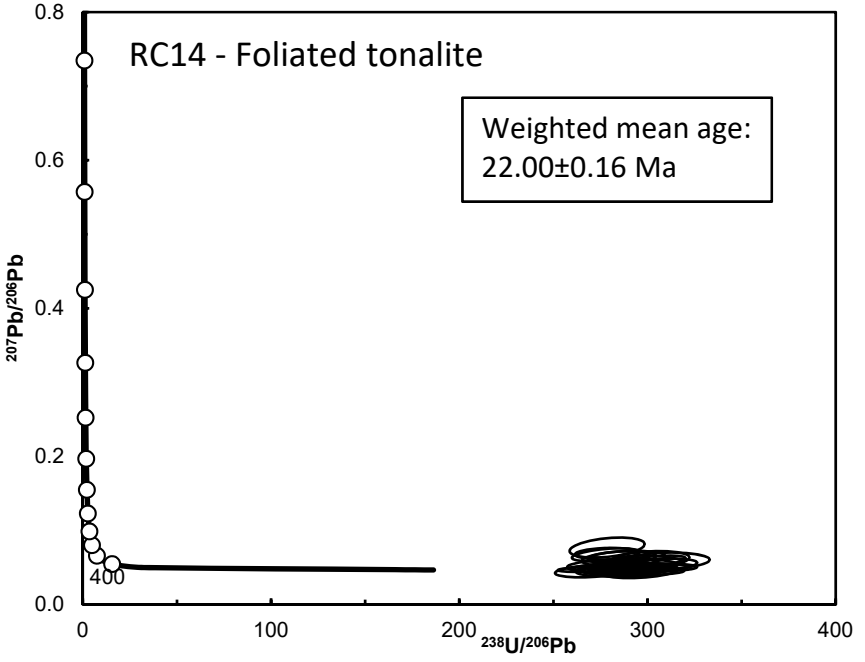

Data-point error ellipses are 2σ

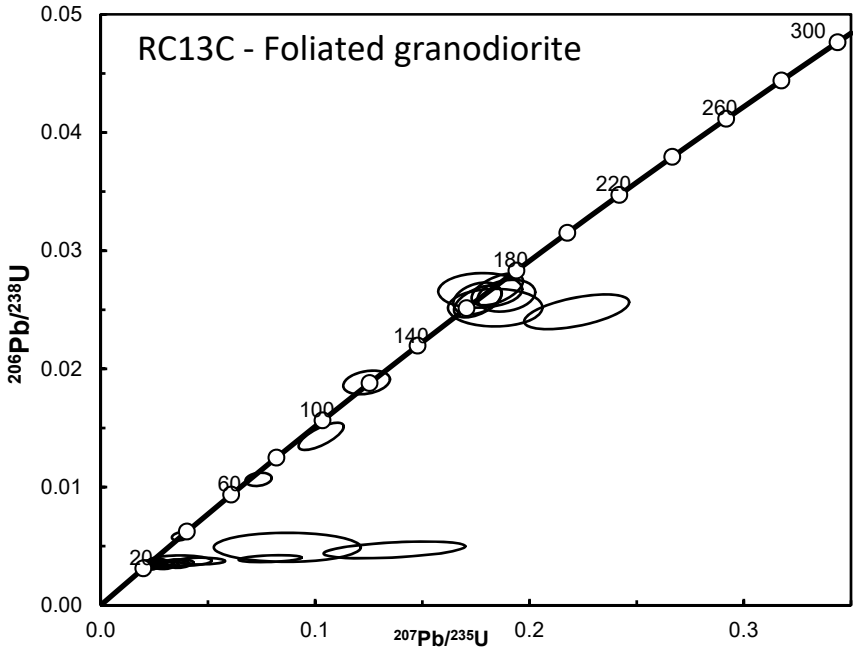

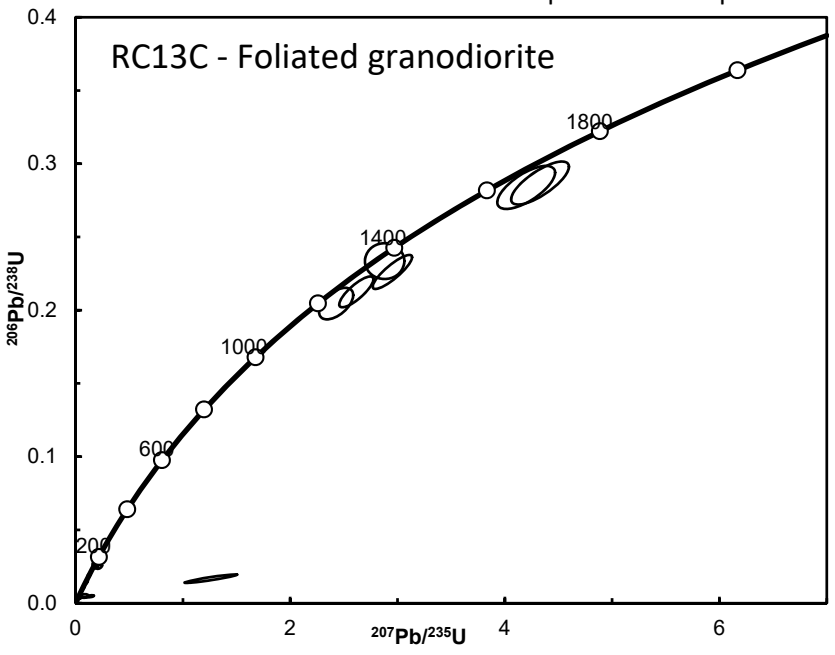

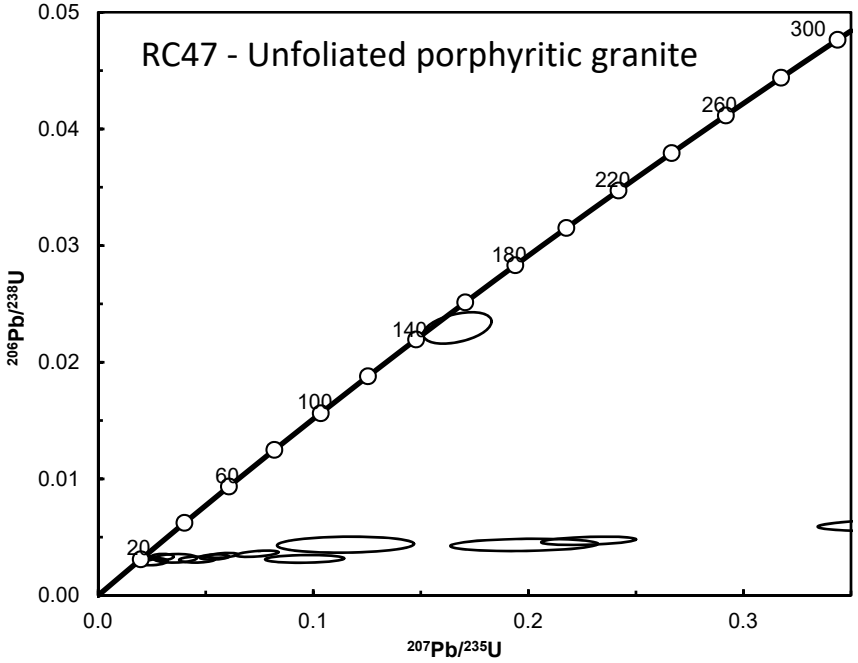

Figure DR7. Weighted mean diagrams of $^{206}Pb/^{238}U$ ages for individual igneous samples from Cemetery Ridge (2 pages of graphs).

Plots created using Isoplot 3.75 (Ludwig, 2012). Error bars represent 2σ propagated errors (Appendix DR1). Analyses are corrected for common Pb using the ^{207}Pb method (Ludwig, 2012).

All analyses except those obviously from inherited grains (Figure DR6) were utilized, including those requiring a large common Pb correction (Figures DR5 and DR6). Twelve analyses total from among the eight samples were rejected by Isoplot as outliers (shown by gray bars). We also calculated weighted mean ages for each sample using only those analyses with the least common Pb contamination. For these calculations, we excluded analysis for which the common Pb correction resulted in a change to the $^{206}Pb/^{238}U$ age of more than 2%. The resultant weighted mean ages were little changed compared to the calculations using all analyses. The average difference between the two methods was 0.04 Ma and the largest difference was 0.10 Ma, in all cases well within the 95% confidence interval.

Samples are arranged from those with relatively more epizonal textures and less well developed foliation at the top of the first page of the figure to those with relatively more mesozonal textures and more strongly developed foliation at the bottom of the second page. Rock type and degree of fabric development are listed on each diagram. See Figure 1B of the main manuscript for sample locations.

References

Ludwig, K.R., 2012, User's manual for Isoplot 3.75: A Geochronological Toolkit for Microsoft Excel: Berkeley Geochronology Center, Special Publication 5, 75 p.

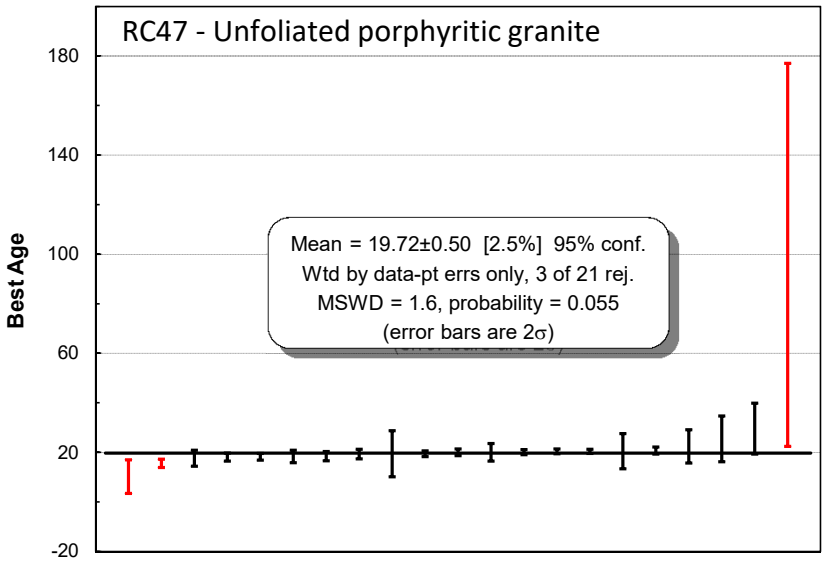
RC47 - Unfoliated porphyritic granite
Best Age
180
140
100
60
20
-20
Mean = 19.72±0.50 [2.5%] 95% conf.
Wtd by data-pt errs only, 3 of 21 rej.
MSWD = 1.6, probability = 0.055
(error bars are 2σ)

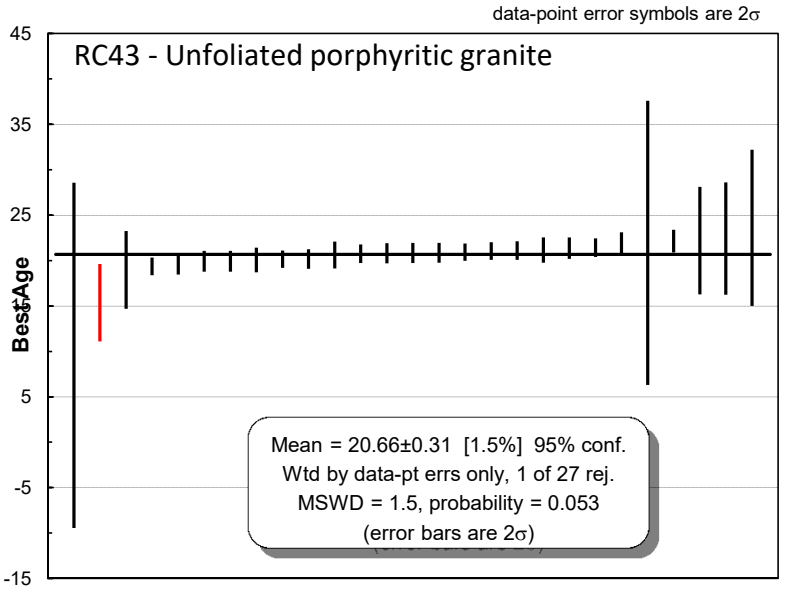
data-point error symbols are 2σ
RC43 - Unfoliated porphyritic granite
Best Age
45
35
25
5
-5
-15
Mean = 20.66±0.31 [1.5%] 95% conf.
Wtd by data-pt errs only, 1 of 27 rej.
MSWD = 1.5, probability = 0.053
(error bars are 2σ)

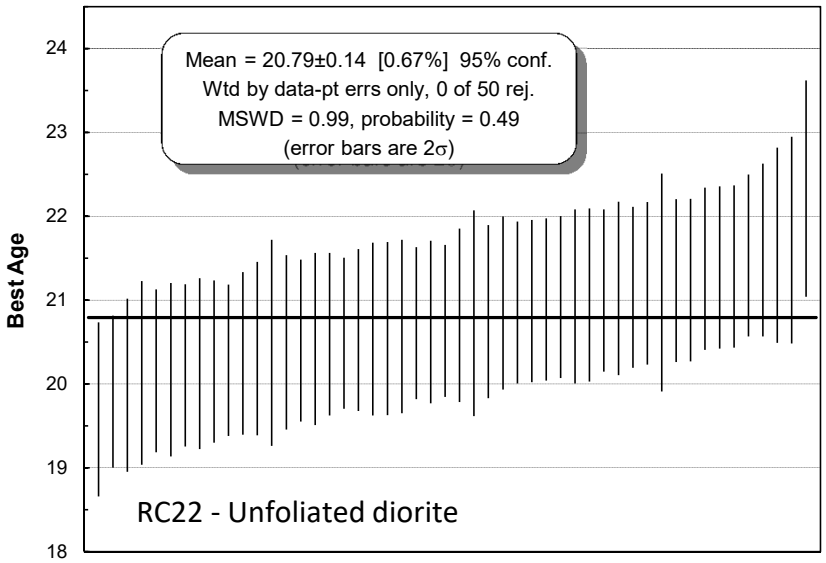
Best Age
24
23
22
21
20
19
18
Mean = 20.79±0.14 [0.67%] 95% conf.
Wtd by data-pt errs only, 0 of 50 rej.
MSWD = 0.99, probability = 0.49
(error bars are 2σ)
RC22 - Unfoliated diorite

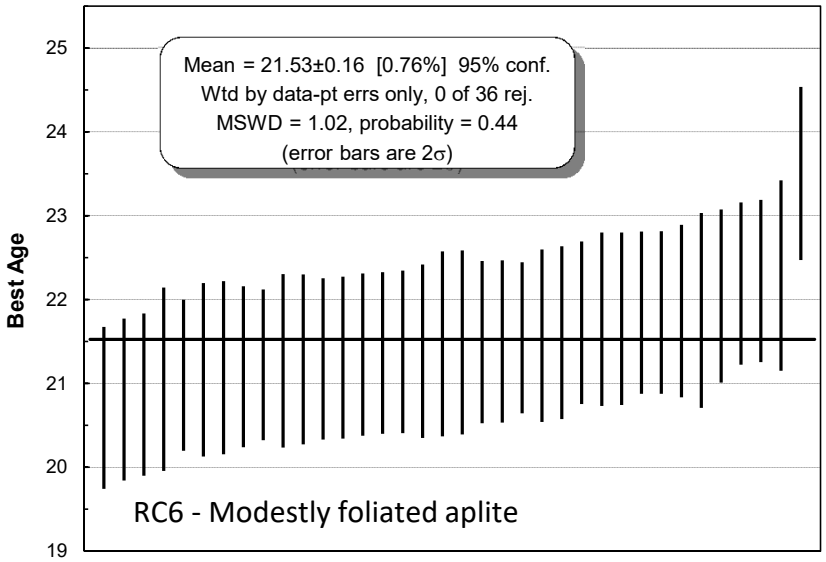
Best Age
25
24
23
22
21
20
19
Mean = 21.53±0.16 [0.76%] 95% conf.
Wtd by data-pt errs only, 0 of 36 rej.
MSWD = 1.02, probability = 0.44
(error bars are 2σ)
RC6 - Modestly foliated aplite

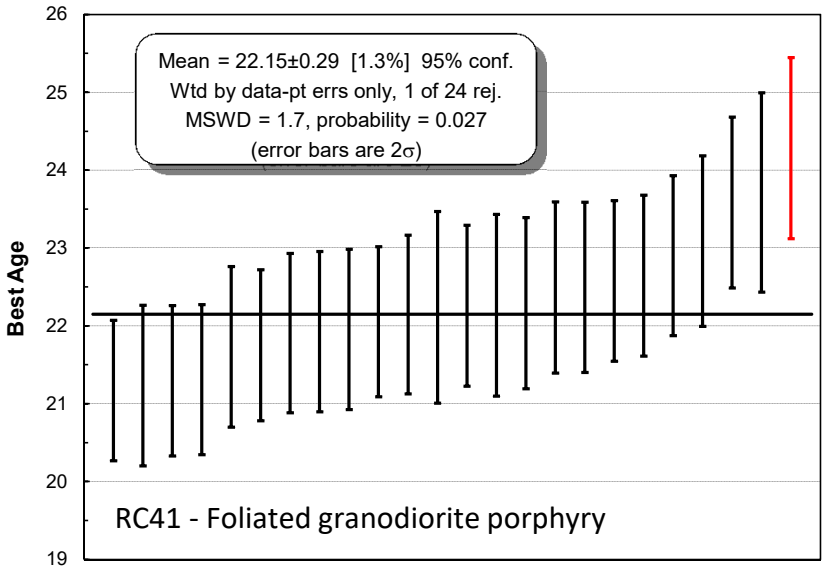
Best Age
26
25
24
23
22
21
20
19
Mean = 22.15±0.29 [1.3%] 95% conf.
Wtd by data-pt errs only, 1 of 24 rej.
MSWD = 1.7, probability = 0.027
(error bars are 2σ)
RC41 - Foliated granodiorite porphyry

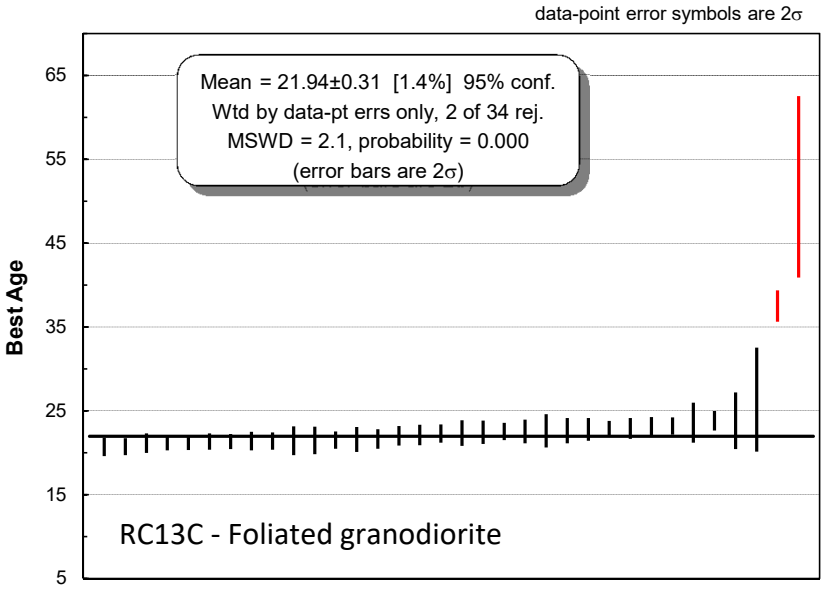
data-point error symbols are 2σ
Best Age
65
55
45
35
25
15
5
Mean = 21.94±0.31 [1.4%] 95% conf.
Wtd by data-pt errs only, 2 of 34 rej.
MSWD = 2.1, probability = 0.000
(error bars are 2σ)
RC13C - Foliated granodiorite

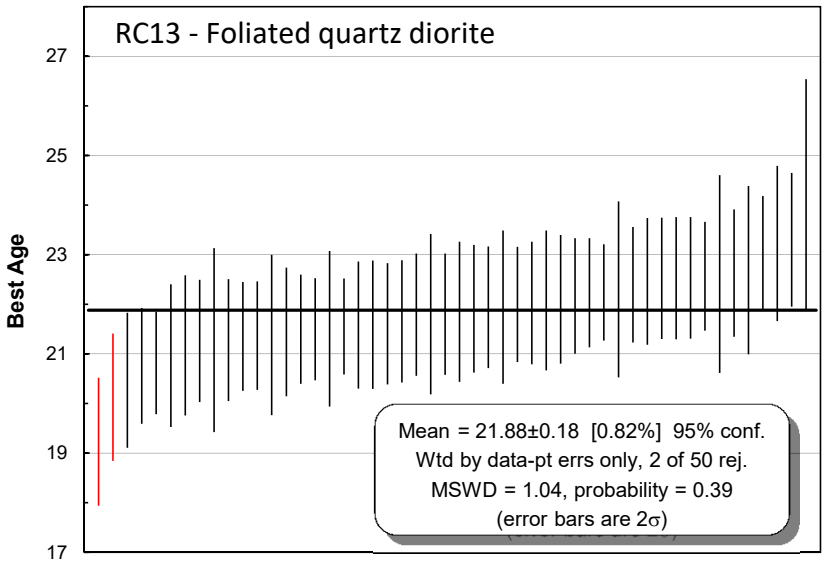
RC13 - Foliated quartz diorite
Best Age
27
25
23
21
19
17
Mean = 21.88±0.18 [0.82%] 95% conf.
Wtd by data-pt errs only, 2 of 50 rej.
MSWD = 1.04, probability = 0.39
(error bars are 2σ)

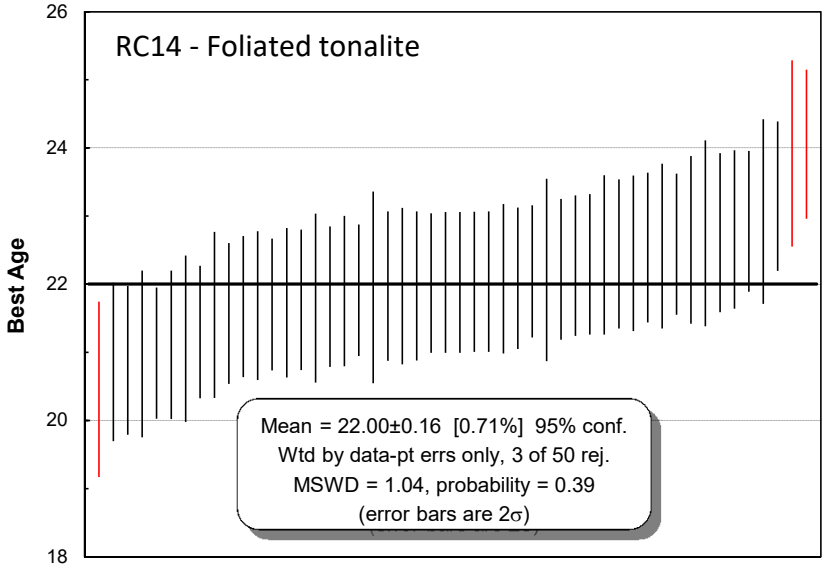
RC14 - Foliated tonalite
Best Age
26
24
22
20
18
Mean = 22.00±0.16 [0.71%] 95% conf.
Wtd by data-pt errs only, 3 of 50 rej.
MSWD = 1.04, probability = 0.39
(error bars are 2σ)